Interaction of 8–46 MeV/nucleon ^{20}Ne with Cu

L. Pieńkowski, J. Jastrzębski, and W. Kurcewicz
Heavy Ion Laboratory and Institute of Experimental Physics, Warsaw University, Warsaw, Poland

A. Gizon
Institut des Sciences Nucléaires, IN2P3-CNRS, Université Joseph-Fourier, F-38026 Grenoble CEDEX, France

J. Blachot and J. Crançon
Département de Recherche Fondamentale, Service de Physique, Centre d'Etudes Nucléaires, F-38041 Grenoble CEDEX, France

(Received 25 July 1990)

Excitation functions and thick-target recoil ranges for radioactive nuclei produced in ^{20}Ne bombardment of natural copper over a 8–46-MeV/nucleon energy range have been measured using the activation technique. From the experimental data the mass yields, charge distributions, total reaction cross section, average and maximum recoil velocities, linear momentum transfer, and excitation energies were deduced. These quantities are compared with similar data on copper obtained using ^{14}N projectiles by our group and lighter ions in other works. In ^{20}Ne-induced reactions the maximum linear momentum transfer in central collisions is reached at a bombarding energy of 11 MeV/nucleon and is equal to 2.8 GeV/c. At the same projectile energy the excitation energy of heavy prefragments produced in these collisions reached the value of about 2 MeV/nucleon. For higher bombarding energies the excitation energy per nucleon slightly increases up to about 2.5 MeV/nucleon. The distribution of the recoil velocity deduced from the present experiment at 30 MeV/nucleon bombarding energy seems to be in contradiction with the results of a Landau-Vlasov simulation of the reaction dynamics.

I. INTRODUCTION

It was observed in a number of previous investigations that in the interaction of light and heavy ions with nuclei the linear momentum transferred from the projectile to the heavy reaction residues[1–3] and the deposited excitation energy[4–6] reach their limiting values near the Fermi energy. Although the phenomenon of this limitation is now well established, at least for fissionable targets, its full understanding is not yet achieved. One may hope that the collection of more systematic data concerning linear momentum transfer (LMT) and energy deposition for various target-projectile combinations may be of some help in the description of the limitation phenomena.

One of the methods currently used[7–12] in the experiments aiming to determine the LMT for light- and intermediate-mass targets is the measurement of the recoil ranges of the heavy reaction residues.[13] Using this method, it was shown that in the $^{4}He+^{59}Co$ reaction[7] the LMT reaches its maximum value of 880 MeV/c at ^{4}He bombarding energy of about 90 MeV. This result was recently confirmed.[14]

In the present work the study of the linear momentum and energy deposition was performed on a target with a mass similar to that used in Ref. 7, but with ^{14}N and ^{20}Ne ions. Therefore, the dependence of the LMT on the projectile mass could be investigated in this mass region. We have taken, however, a natural Cu rather than a ^{59}Co target. This was dictated by a clear preference for this target in a number of previous radiochemical studies with light projectiles at intermediate and high bombarding energies,[15–20] heavy ions at GeV bombarding energies[4,17,18,21–24] and also pions[19,25,26] and gamma rays.[27] Recently, the reactions of heavy ions at some selected intermediate energies were also investigated with this target.[9,28–31]

The present experiment consisted in the determination of the thick-target recoil ranges of the radioactive reaction products and their production cross section for the ^{14}N and ^{20}Ne projectile at a number of bombarding energies between 8 and 46 MeV/nucleon. At each bombarding energy, the recoil velocities were deduced from the recoil ranges under certain assumptions which are discussed in some detail. From the cross section of the radioactive residues, a complete mass distribution of heavy reaction products was deduced using a by now well-established fitting procedure, first proposed by Rudstam[15] and subsequently used and extended by a number of investigators.[17,20,28] By folding the mass distribution with the distribution of the recoil velocities as a function of the product mass, the average LMT at each bombarding energy was deduced. Similarly, as in the $^{4}He+^{59}Co$ reaction, a "saturation" of the recoil velocities for the reaction products lighter than and far removed from the target was observed. This saturation velocity indicates the existence of a maximum LMT for each bombarding energy, presumably related to the most central collisions in the $^{20}Ne+^{nat}Cu$ reactions. The maximum recoil velocity is compared with some model calculations. The average and maximum excitation energy of heavy reaction residues before the evaporation process are deduced from their kinematic properties. Additionally, the mass distribution obtained from the experiment is used as an independent observable in the determination of this average excitation energy.

In the beginning of this work, the ^{14}N projectile was used for a few bombarding energies. Later, ^{20}Ne ions were selected in order to get information about LMT with the heaviest available projectile which does not produce an appreciable radioactivity when interacting with the catcher material. It is the ^{20}Ne+^{nat}Cu reaction which is described in the present paper in detail. The ^{14}N+^{nat}Cu data are only summarized and used occasionally whenever the projectile dependence of the measured quantities is considered worth presenting. Preliminary results of the present work were previously published.[8,32,33]

II. EXPERIMENTAL TECHNIQUE

The target stack we used consisted of a catcher foil, a natural Cu target, 10–50 mg/cm^2 thick, and a second catcher foil. Catcher foils were either carbon or aluminum. The purity of all materials used was better than 99.99%. The target stack was bombarded with 8–46-MeV/nucleon ^{20}Ne beams. Heavy reaction products (recoil nuclei) were stopped either in the Cu target or in the catcher foils. The catcher foil thickness was at least twice the range of the recoils expected for the full momentum transfer. After irradiation the analysis of gamma-ray activity of target and catcher foils has been performed. This experimental technique is known as "thick-target–thick-catcher recoil range measurement."[13]

Up to three target stacks have been used during a single run. The target stacks were separated by aluminum foils to obtain the desired beam energy. Additional aluminum or carbon foils made from the catcher materials have been inserted upstream to monitor the purity of the catcher foils. Beam intensity was measured using a calibrated Faraday cup placed close to the target assembly. A full ionization of the ^{20}Ne beam after its passage through the thick-target–catcher material was assumed. In addition, for energies around 20 MeV/nucleon, the beam intensity was checked by measuring the absolute activities of ^{22}Na and ^{24}Na isotopes, produced in the monitor foils. The cross section for the production of these isotopes with a ^{20}Ne beam of 20 MeV/nucleon interacting with Al and C targets was recently reported.[34]

Target thicknesses, beam energies, and the list of experiments are given in Table I. The energy-loss tables[35] were used to calculate the beam energy inside the target. The beam energy uncertainty was estimated assuming 5% uncertainty in the energy-loss tables. The incident beam energy error was assumed negligible.

Experiments 1–4 were performed on the SARA facility (ISN, Grenoble), while experiment 5 was run on the SC synchrocyclotron (CERN, Geneve). Irradiation times ranged from 15 min to a few hours, with beam current of the order of 10^{11} ions/s. Two identical target setups have been used during experiments 1 and 2. One of them was bombarded for 15 min, while another was bombarded for 3 h. The gamma activity measurements have been started from 30 min to a few hours after irradiation and were continued over a period of a few months (in Grenoble and Warsaw). For each target and catchers five to ten measurements were completed. The Ge(Li) detectors having 5–25 % efficiency and 1.8–3.5-keV resoluton at 1.3 MeV gamma-ray energy were used. The resulting gamma-ray spectra have been analyzed with computer programs SPECFIT[36] (in Grenoble) and ACTIV[37] (in Warsaw). The identification of the radioactive nuclei and activity determination were based on known decay data.[38]

TABLE I. Experimental conditions.

Experiment number	Target thickness (mg/cm^2)	Beam energy in the middle of the target[a] (MeV/nucleon)	Half of the beam energy loss in the target (MeV/nucleon)
1	19.2	8.7(1)	1.4
2	10.8	10.8(5)	0.7
3	13.4	14.3(8)	0.7
2	14.7	15.0(3)	0.8
2	16.7	18.8(1)	0.7
3	13.4	22.7(4)	0.5
4	19.3	24.1(3)	0.7
5	53.8	28.6(10)	1.7
4	16.7	28.7(1)	0.5
3	13.4	29.2(1)	0.4
5	53.8	37.1(6)	1.4
5	53.8	46.1(2)	1.2

[a]Numbers in parentheses represent uncertainties in the last significant digits.

III. EXPERIMENTAL RESULTS

From the analysis of the gamma-ray spectra of the radioactive reaction products in the target and forward and backward catchers, their production cross sections as a function of the ^{20}Ne bombarding energy were obtained. These cross sections are listed in Table II and are shown for some selected products in the upper part of Fig. 1. The quoted errors do not take into account the uncertainty of the beam current determination (estimated to be about 10%) as well as the energy spread in the target. The last uncertainty is only important for the cross sections which change appreciably during the beam energy degradation in the target material. In the most critical cases (as, e.g., ^{69}Ge at 10–25 MeV/nucleon), this error may attain 25%.

Table III and the lower part of Fig. 1 show the quantity FW determined from the measured gamma-ray intensities. Here F is the activity ratio of a given reaction product in the forward catcher to the total activity of this product, and W is the target thickness. As it was shown in Ref. 21 and will be also discussed in the following section, under certain assumptions the FW quantity represents, with good approximation, the forward component of the average recoil range.

Similarly as the quantity F, the quantity B is defined as the activity ratio of a given reaction product in the backward catcher to the total activity of this product. For the

TABLE II. Cross sections (in mb) for $^{20}Ne + ^{nat}Cu$ reaction products of the type C cumulative or I independent. Numbers in parentheses represent uncertainties in the last significant digits.

Product	Beam energy in laboratory system (in MeV/nucleon)												Type
	8.7	10.8	14.3	15.0	18.8	22.7	24.1	28.6	28.7	29.2	37.1	46.1	
^{77}Kr	9(3)												C
^{76}Kr	9.8(8)	3.6(4)											C
$^{77}Br^{g}$	17.2(19)	5.3(6)	<0.1										C
$^{76}Br^{g}$	22(10)	<5.0	<0.25										I
^{75}Br	36(3)												C
^{75}Se	50(15)	25(1)	1.5(8)	<2.0									C
^{73}Se	60.5(35)	36(2)	2.7(6)	3.2(3)	0.32(2)	0.12(2)	<0.6			<0.1			C
^{72}Se	40(2)	8(3)											C
^{74}As	2.5(1)	1.8(5)											I
^{71}As	88(3)	50(8)	18.7(35)	15.1(8)	1.8(1)	0.42(4)	0.27(4)	<0.3	<0.3	0.23(7)		<0.1	C
^{70}As	47(5)	43(5)											C
^{69}Ge	62(3)	93(6)	28(5)	31.5(25)	6.8(5)	1.31(19)	0.78(7)	<0.8	0.33(15)	0.26(3)		<0.1	C
^{68}Ge	55(3)			28(7)									C
^{67}Ga	85(6)	160(30)	76(8)	95(4)	34(1)	8.8(9)	9.0(4)	5.6(8)	3.2(4)	2.4(5)	2.3(3)	0.67(7)	C
^{66}Ga	51(2)	120(25)		80(15)	38(3)		10.5(9)		5.0(5)				C
^{65}Zn	106(10)	180(12)	160(15)	187(9)	130(5)	55.3(25)	62.2(13)	47.6(27)	37.6(8)	35.5(25)	27(2)	16.0(5)	C
^{62}Zn	2.5(3)	9(2)	12(2)	15(1)	16(1)	9.8(9)	11.2(20)	10(2)	7.85(60)	7.5(6)	6.0(8)	5.6(10)	C
^{64}Cu	60(20)	85(25)	72(15)	91(7)	99(9)	79(8)		89(10)	107(10)	93(10)	70(9)	80(9)	I
^{61}Cu	16.7(30)	73(12)	55(6)		88(8)	56.7(40)	57.7(40)		49.1(40)	52(5)	44(5)	44(4)	C
^{57}Ni	0.24(6)	<0.8	1.3(2)	1.8(1)	2.9(2)	2.7(2)	3.28(41)	3.2(2)	3.3(5)	3.4(3)	2.7(2)	2.6(2)	C
^{56}Ni	<0.1		<0.1	<0.1	0.15(4)			<0.3	0.27(8)	0.20(6)	<0.2	<0.3	C
^{60}Co	2.8(3)	12(1)	13(1)	18.8(15)	23.7(11)	21.1(7)		24.2(18)	25.7(26)	21.8(15)	24(2)	22(4)	C
^{58}Co	16.8(10)	42(2)	81(7)	98.4(15)	100(8)	110(5)	116(3)	124(10)	118(5)	112(7)	105(8)	87(9)	I
^{57}Co	13(5)	22.5(30)	74(8)	90(2)	105(10)	102(7)	120(4)	117(12)	131(9)	117(9)	100(9)	78(10)	I
^{56}Co	2.6(3)	6.0(3)	13(1)	15.9(8)	27.8(21)	30.6(11)	35.0(7)	34(4)	28.4(50)	28(2)	30(2)	25.5(10)	I
^{55}Co	0.25(3)	<1.5	1.9(2)	2.2(2)	3.7(1)	4.45(40)	5.5(10)	5.6(4)	4.8(4)	5.4(5)	4.6(4)	4.5(4)	C
^{59}Fe	<0.15		1.1(2)	1.6(2)	2.6(2)	2.1(2)	2.8(4)	2.7(2)	3.0(4)	2.9(4)	3.1(2)	3.2(2)	C
^{52}Fe					<0.1	0.30(5)	0.20(5)		0.44(6)	0.32(3)	0.43(4)	0.45(15)	C
^{56}Mn	0.46(9)	<1.5	2.0(2)		5.2(7)	4.6(8)	5.81(12)		6.0(6)	5.6(3)	8(3)	10(4)	C
^{54}Mn	7.0(9)	13.0(5)	30(1)	35.5(5)	67.4(9)	68.6(11)	86.3(46)	86(4)	89(3)	79(8)	80(5)	66.4(8)	I
^{52}Mn	1.93(10)	4.5(5)	11(1)	13.0(7)	25.0(6)	35.7(8)	38.1(17)	45(3)	41(3)	47.5(50)	40(3)	34.5(34)	I
^{51}Cr	5.7(14)	7.6(6)		25.5(15)	59.4(21)	70(5)	96.4(22)	97(5)	90(8)	78(5)	90(8)	89(10)	C
^{48}Cr			0.11(2)		0.31(6)	0.61(6)	0.6(1)	0.72(8)	1.0(2)	0.95(10)	1.0(1)	1.15(10)	C
^{48}V	2.01(16)	3.3(1)	7.5(7)	7.0(7)	15(1)	27.0(9)	33.1(8)	36.8(22)	45(2)	44.5(50)	43.7(17)	39(2)	C
^{48}Sc	<0.5	<0.2	<0.1	<0.3	<0.3	0.4(1)			<0.1		<0.3	<2.2	I
^{47}Sc	0.37(5)	<0.4	0.9(1)	0.9(2)	1.9(4)	3.28(27)	4.0(5)	5.0(6)	5.3(6)		6.7(7)	7.6(14)	C
^{46}Sc	1.3(2)	1.4(5)	3.4(3)	3.2(2)	6.56(33)	12.3(8)	14.1(4)	17(1)	18.5(20)	18.9(10)	23(2)	22.2(8)	I
$^{44}Sc^{g}$	<0.6		0.7(4)	<1.0		3.4(4)	<4.5		5.6(5)	6.9(4)	<2.0	<8.0	C
$^{44}Sc^{m}$	1.55(11)	1.8(2)	3.8(6)	3.8(5)	7.2(6)	13.2(10)	14.9(4)	17.5(10)	20.2(25)	18.5(12)	24(2)	26.3(17)	I
^{43}K			0.31(8)	0.35(9)	0.58(6)	1.03(15)	1.4(1)	1.7(1)	2.0(2)	1.8(2)	2.3(2)	3.0(3)	C

reaction products observed in the present work, the backward recoils were very small and their precise determination was not attempted. We have only determined the lower limit of the ratio $F/B \geq 80$. This limit is in good agreement with other heavy-ion data with a ^{nat}Cu target at intermediate bombarding energies.[9,21,29,39]

IV. DATA ANALYSIS

A. Mass-yield distribution

To estimate the total cross section for heavy fragment production σ_{HR}, to calculate the mean mass of the reac-

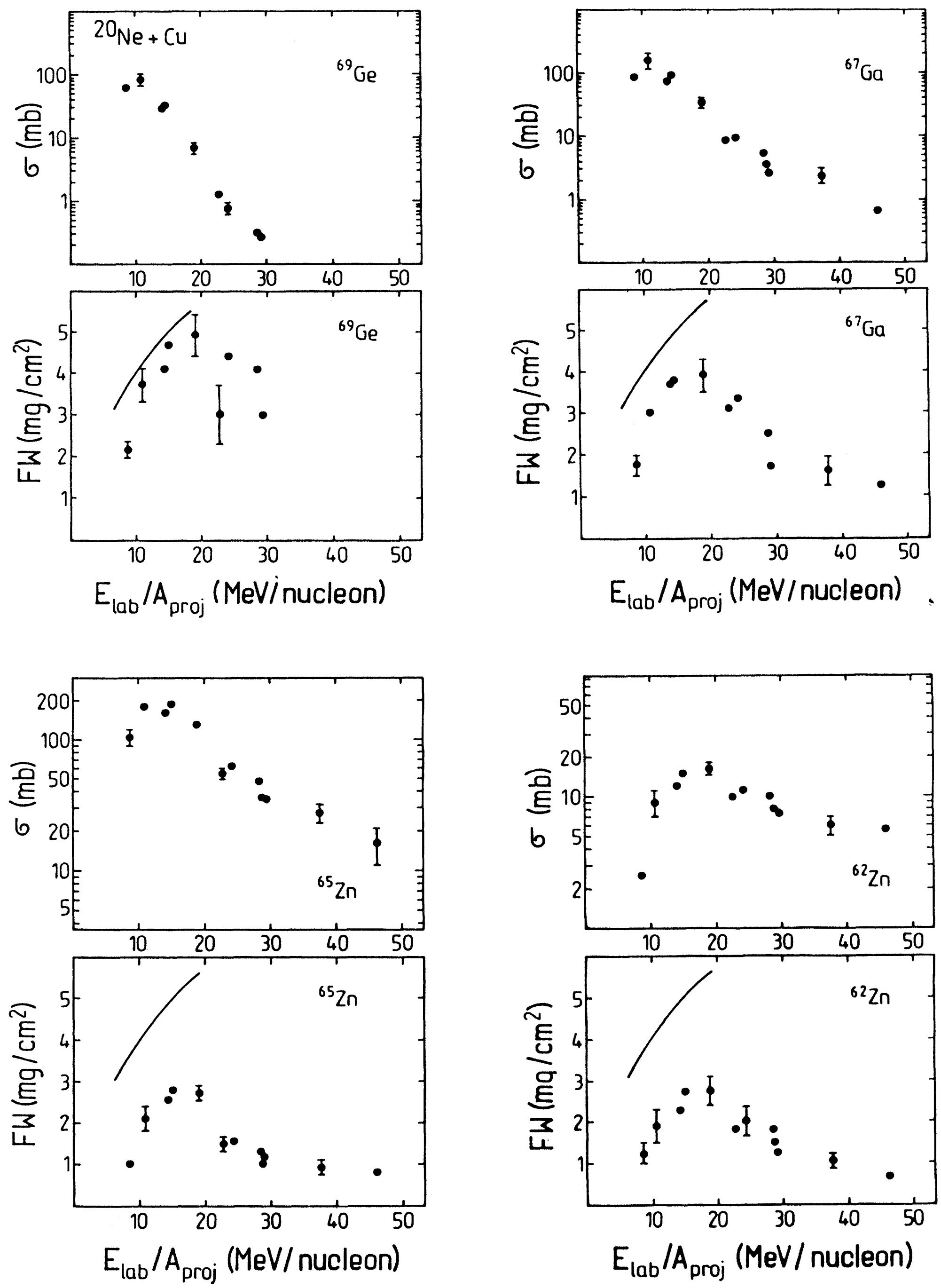

FIG. 1. Cross section σ and the fraction of the total activity collected on the forward catcher times the target thickness FW for the radioactive nuclei produced from ^{20}Ne bombardment of the ^{nat}Cu target as a function of ^{20}Ne energy per nucleon. The curves represent the calculated FW values with the assumption of a full momentum-transfer reaction to the compound nucleus.

tion products $\langle A_{prod} \rangle$, and their average parallel velocity component $\langle v_{\parallel} \rangle$, it is necessary to know the mass distribution $\sigma(A)$ of the reaction products. Since the radioactive nuclei observed in the present work represent only a fraction of the total cross section for the production of heavy reaction residues, one has to assume some functional relationship concerning $\sigma(A)$, and to use a minimization procedure to adjust the relevant parameters. Such a methodology has been used frequently[9,15,17,28]—the method chosen in this work is very similar to the one used by Lund *et al.*[28] We have found the approach of Lund *et al.* very appealing due to the explicit use of the factorization of the cross-section formula on two terms. The first term describes the charge dispersion curve and the second one the variation of the cross section with the product mass number. It has been assumed that the cross

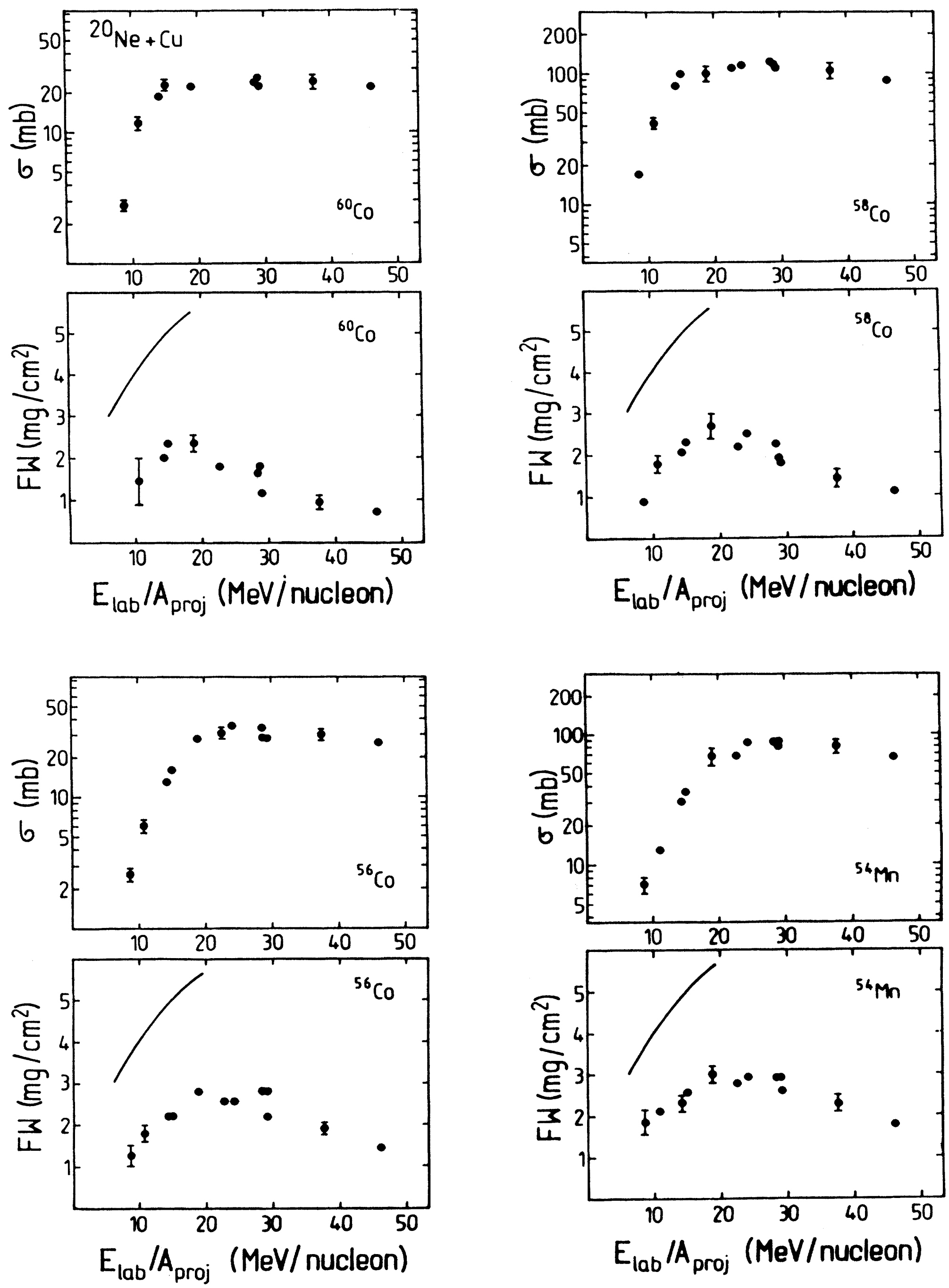

FIG. 1. (*Continued*).

section of a product with mass A and charge Z can be factorized by two functions:

$$\sigma_F(A,Z)=P(Z_P-Z)\sigma_F(A)\ , \tag{1}$$

where $P(Z_P-Z)$ is the charge dispersion, $\sigma_F(A)$ the mass distribution, Z_P the most probable charge for a given A, and subscript F indicates the functional form. The function (1) is to be minimized in respect to the experimentally determined set of cross sections $\sigma(A,Z)$ of the radioactive reaction products. The charge distribution for a given mass is assumed to be a Gaussian:

$$P(Z_P-Z)=\frac{1}{\sqrt{2\pi}\,s}\exp\left[-\frac{(Z_P-Z)^2}{2s^2}\right]\ , \tag{2}$$

where the full width at half maximum (FWHM)≈ 2.354 s and Z_P depends linearly on the mass number:

$$Z_P=a_0+a_1A\ . \tag{3}$$

The linear dependence (3) of Z_P on A is different from

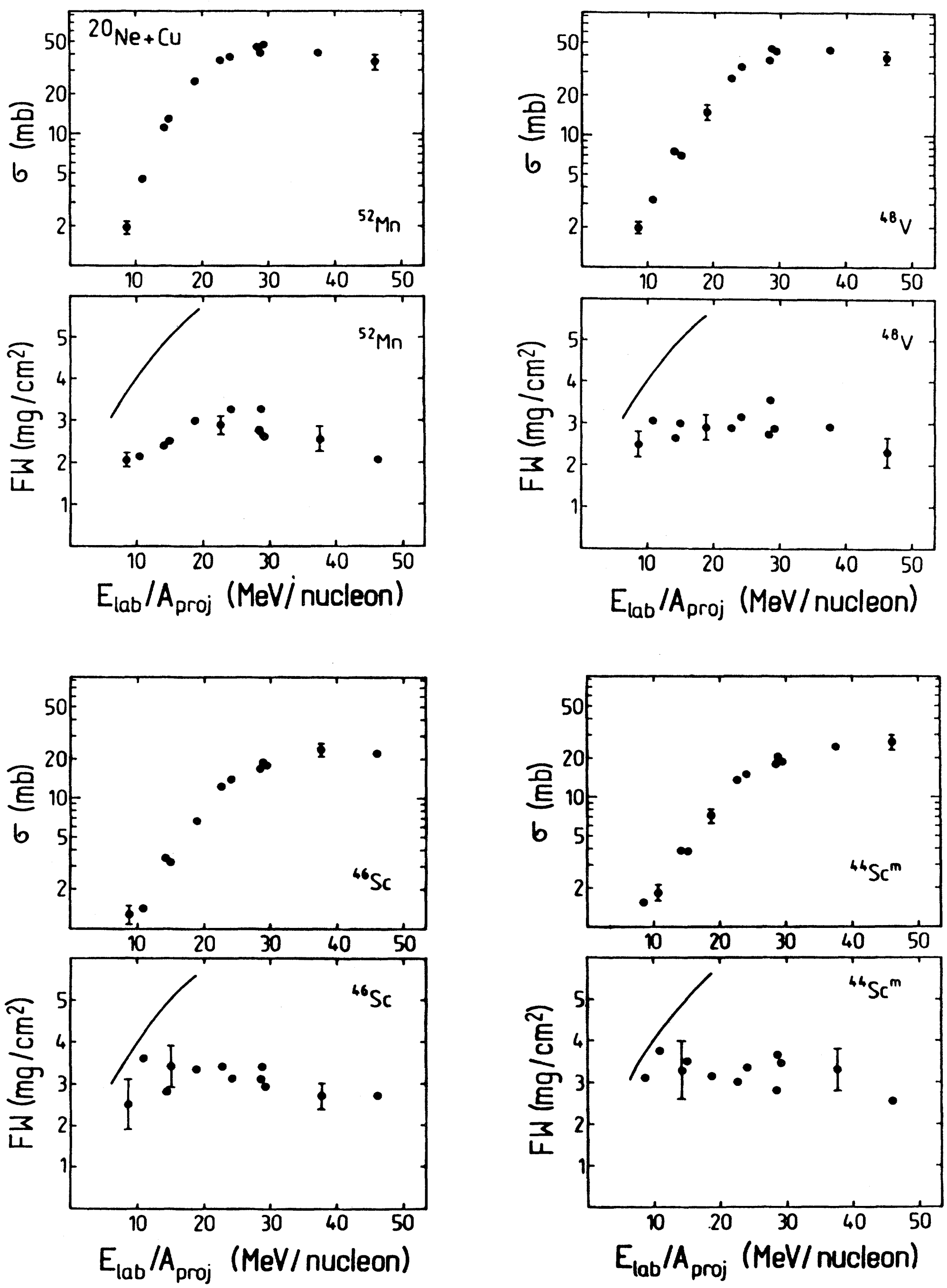

FIG. 1. (*Continued*).

that used by Lund *et al.*, where the A dependence of Z_P was quadratic:

$$Z_P = a_0 A + a_1 A^2 \,. \tag{4}$$

Our set of data can be fitted by either linear (3) or quadratic (4) functions with no statistically significant difference in the fit quality. It is further assumed that the mass distribution can be approximated by the simple exponential function of A:

$$\sigma_F(A) = \exp(\alpha_0 + \alpha_1 A + \alpha_2 A^2 + \alpha_3 A^3) \,, \tag{5a}$$

or by a slightly more complicated functional form:

$$\sigma_F(A) = \frac{\exp[\alpha_1 + \alpha_2(\alpha_0 - A) + \alpha_3(\alpha_0 - A)^2]}{1 + \exp[\alpha_4(\alpha_0 - A)]} \,. \tag{5b}$$

At bombarding energy below 18 MeV/nucleon, no significant change of the fit quality and parameters influencing $P(Z_P - Z)$ has been observed, whichever of the functional forms listed above was used. At beam energy above 18 MeV/nucleon, a good quality fit was obtained only with $\sigma_F(A)$ postulated in the formula (5b). This formula is able to account for a sharp drop of the cross section for the products with mass number higher than the target mass. Such a drop is apparently present in the ^{20}Ne+Cu reaction at bombarding energies above 18 MeV/nucleon and is discerned here by our fitting procedure. A similar sharp decrease of the cross section for the transtarget nuclei was recently observed in the ^{20}Ne+^{60}Ni reaction at 37 MeV/nucleon.[40] In that work the mass distribution was obtained from the in-beam and radioactivity gamma-ray measurements, without any

TABLE III. FW parameter (in mg/cm^2) for ^{20}Ne+$^{\mathrm{nat}}$Cu reaction products. Numbers in parentheses represent uncertainties in the last significant digits.

	Beam energy in laboratory system (MeV/nucleon)											
Product	8.7	10.8	14.3	15.0	18.8	22.7	24.1	28.6	28.7	29.2	37.1	46.1
^{77}Kr	8.7(22)											
^{76}Kr	7.5(3)	5.4(11)										
^{77}Br^g	6.6(8)	6.1(12)										
^{76}Br^g	7.3(5)											
^{75}Br	6.1(6)											
^{75}Se	4.8(2)	5.1(5)	3.2(14)									
^{73}Se	4.9(4)	4.35(51)	3.5(9)	5.5(9)	4.18(45)	2.7(7)						
^{72}Se	3.1(2)	4(2)										
^{74}As	3.5(5)	4.8(27)										
^{71}As	4.06(26)	3.2(7)	3.9(7)	5.1(5)	4.3(4)	3.5(5)	4.3(17)			3.5(15)		
^{70}As	3.0(4)	3.5(6)										
^{69}Ge	2.14(16)	3.7(4)	4.1(8)	4.7(6)	4.9(5)	3.0(7)	4.4(14)		4.1(21)	3.0(7)		
^{68}Ge	2.52(48)			5.0(18)								
^{67}Ga	1.76(14)	3.0(8)	3.7(5)	3.82(24)	3.9(4)	3.1(5)	3.33(33)	3.8(8)	2.48(38)	1.73(56)	1.66(35)	1.24(22)
^{66}Ga	1.13(9)	2.7(8)			3.7(4)		3.7(15)		2.0(7)			
^{65}Zn	1.00(14)	2.1(3)	2.56(18)	2.78(21)	2.72(17)	1.52(11)	1.55(5)	1.55(15)	1.02(9)	1.13(13)	0.92(9)	0.81(4)
^{62}Zn	1.23(21)	1.9(4)	2.30(42)	2.75(29)	2.74(25)	1.82(15)	1.98(37)	1.8(3)	1.51(12)	1.25(25)	1.06(16)	0.63(8)
^{64}Cu	<1.5	1.9(8)	1.62(40)	2.58(34)	1.1(3)	0.80(15)		0.53(10)	0.62(15)	0.50(9)	0.26(13)	0.12(5)
^{61}Cu	0.76(16)	1.95(55)	2.26(31)		2.31(24)	1.60(18)	2.13(18)		1.50(12)	1.03(14)	0.74(12)	0.49(6)
^{57}Ni	0.96(47)		1.7(4)	2.01(19)	2.68(29)	2.23(26)	2.70(45)	2.6(3)	2.33(47)	1.59(17)	1.78(25)	1.40(20)
^{56}Ni									3.1(11)	3.5(13)		
^{60}Co	<1.4	1.44(55)	2.00(15)	2.35(27)	2.34(17)	1.80(9)		1.65(20)	1.8(11)	1.14(12)	0.95(7)	0.73(12)
^{58}Co	0.92(8)	1.80(15)	2.07(18)	2.31(6)	2.7(3)	2.19(16)	2.51(13)	2.27(50)	1.90(19)	1.76(17)	1.42(12)	1.09(9)
^{57}Co	1.3(7)	1.92(32)	2.17(31)	2.51(10)	2.9(3)	2.35(5)	2.65(35)	2.41(8)	1.90(28)	1.96(24)	1.61(3)	1.16(10)
^{56}Co	1.26(27)	1.80(20)	2.19(24)	2.21(18)	2.79(33)	2.59(15)	2.60(29)	2.80(40)	2.76(54)	2.18(25)	1.89(4)	1.45(8)
^{55}Co	2.0(3)		2.23(34)	1.83(24)	2.70(12)	2.35(33)	2.5(6)	2.90(33)	2.77(29)	1.94(43)	2.37(27)	1.64(19)
^{59}Fe			2.16(39)	2.47(49)	2.55(31)	2.0(3)	1.5(4)	1.95(23)	1.76(40)	1.61(29)	1.28(25)	0.90(18)
^{52}Fe						2.82(74)	4.5(15)		3.04(56)	3.1(5)	3.0(9)	1.6(4)
^{56}Mn	2.5(13)		3.1(15)		2.64(56)	2.50(69)	3.52(21)		2.9(4)	2.09(37)		2.5(5)
^{54}Mn	1.84(31)	2.08(12)	2.32(10)	2.57(6)	3.0(2)	2.77(11)	2.93(24)	2.87(35)	2.86(21)	2.54(41)	2.28(17)	1.73(5)
^{52}Mn	2.05(12)	2.16(34)	2.39(26)	2.52(21)	3.00(7)	2.87(10)	3.28(26)	2.75(30)	3.25(25)	2.60(34)	2.56(29)	2.06(26)
^{51}Cr	2.0(6)	2.13(86)		2.66(25)	2.87(16)	2.98(34)	3.14(16)	2.73(22)	3.1(4)	2.94(22)	2.8(5)	1.76(32)
^{48}Cr			2.1(5)		2.7(8)	3.1(5)	3.4(6)	3.0(5)	3.97(52)	3.1(5)	3.25(60)	3.31(81)
^{48}V	2.5(3)	3.11(25)	2.65(36)	3.0(5)	2.9(3)	2.87(15)	3.15(20)	2.73(26)	3.56(22)	2.82(34)	2.88(32)	2.29(35)
^{48}Sc						3.1(12)						
^{47}Sc	2.6(6)		2.9(9)	4.2(23)	3.7(12)	3.19(42)	3.37(51)	2.85(40)	3.04(22)		2.57(39)	2.4(5)
^{46}Sc	2.5(6)	3.6(5)	2.8(3)	3.4(4)	3.34(27)	3.38(35)	3.10(13)	3.10(23)	3.41(45)	2.93(25)	2.71(16)	2.70(15)
^{44}Sc^g			2.9(9)			3.1(6)			3.23(56)	2.44(34)		
^{44}Sc^m	3.1(7)	4.2(13)	3.28(65)	3.5(7)	3.21(11)	3.01(36)	3.34(18)	2.81(25)	3.66(48)	3.45(32)	3.56(51)	2.56(22)
^{43}K			3.0(8)	3.8(15)	3.46(57)	3.7(9)	4.13(73)	2.9(3)	4.28(86)	3.2(4)	3.02(38)	2.72(33)

fitting procedure.

For the minimization procedure of function (1), we have been using the global set of experimental data rather than only A chains for which the cross section of more than one isobar was experimentally determined.[28] This minimization gives simultaneously the parameters of $P(Z_P-Z)(s,a_0,a_1)$ and of $\sigma_F(A)(\alpha_0,\ldots,\alpha_n)$. Once the minimization procedure is completed, however, the knowledge of one independent or cumulative isobar experimental cross section $\sigma(A,Z)$ and of the $P(Z_P-Z)$ function is sufficient to determine the total cross section of a given mass:

$$\sigma(A)=\frac{\sigma^I(A,Z)}{P(Z_P-Z)} \quad \text{or} \quad \sigma(A)=\frac{\sigma^C(A,Z)}{\sum\limits_{\beta\ \text{chain}} P(Z_P-Z_i)}\ , \tag{6}$$

where $\sigma^I(A,Z)$ and $\sigma^C(A,Z)$ means independent and cumulative experimental cross section, respectively.

To illustrate the results of the fitting procedure, we show in Fig. 2 some typical charge distributions. Their width is a slowly increasing function of the beam energy, as shown in Fig. 3. The dependence of the most probable charge Z_P on the mass number A is almost the same over the investigated beam energy range and is given by the following relationship:

$$Z_P=(0.451A+0.88)\pm0.1 \quad \text{for } A\approx 40-80\ . \tag{7}$$

For the fitting procedure described above one needs the independent cross sections, but most of the experimental data are available as the cumulative cross sections, instead, defined by

$$\sigma^C(A,Z)=\sum_{\beta\ \text{chain}}\sigma^I(A,Z_i)\ . \tag{8}$$

However, if for a given A number for all terms in (8) Z_P-Z_i are of the same sign, then (with errors smaller than the experimental uncertainties of the measured cross section) one has

$$\sigma^C(A,Z)=\sigma^I(A,Z)\ . \tag{9}$$

This results from the narrow charge distributions (Fig. 2). Iteratively, it has been ascertained that the cumulative cross sections for the production of some radionuclides, namely, ^{77}Br, ^{75}Se, ^{65}Zn, do not fulfill this condition, and so the pertaining data have been rejected while determining $\sigma_F(A,Z)$ parameters. Additionally, we observe that if the condition $|Z_P-Z|>0.3$ is fulfilled, then equality (9) is exact within 1%.

Figure 4 presents the deduced mass distribution for a set of beam energies. If, for a given mass number A, more than one isobar cross section was measured, the cross section $\sigma(A)$ is a weighted average of the results obtained from the formula (6). A smooth mass distribution was obtained for all bombarding energies. The only point systematically deviating from a smooth trend is the $A=64$ mass, which was deduced from the cross section of ^{64}Cu. Besides the evaporation from the composite sys-

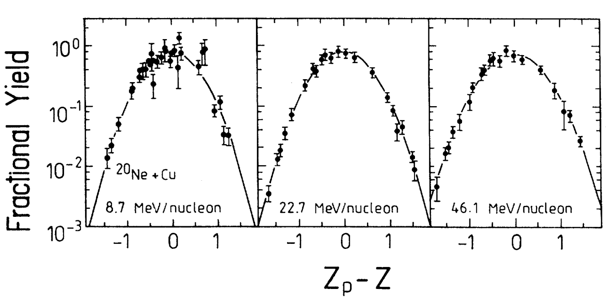

FIG. 2. Charge distribution deduced from the experimentally determined cross section of the radioactive products in the reaction ^{20}Ne+^{nat}Cu at three selected beam energies.

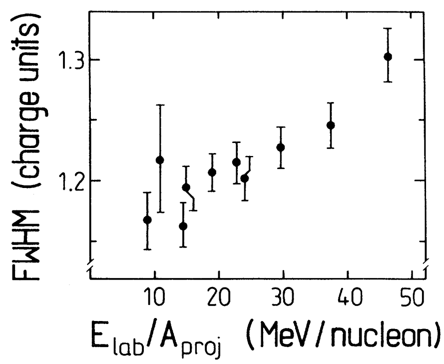

FIG. 3. Width of the charge distribution (see Fig. 2) as a function of the projectile energy per nucleon.

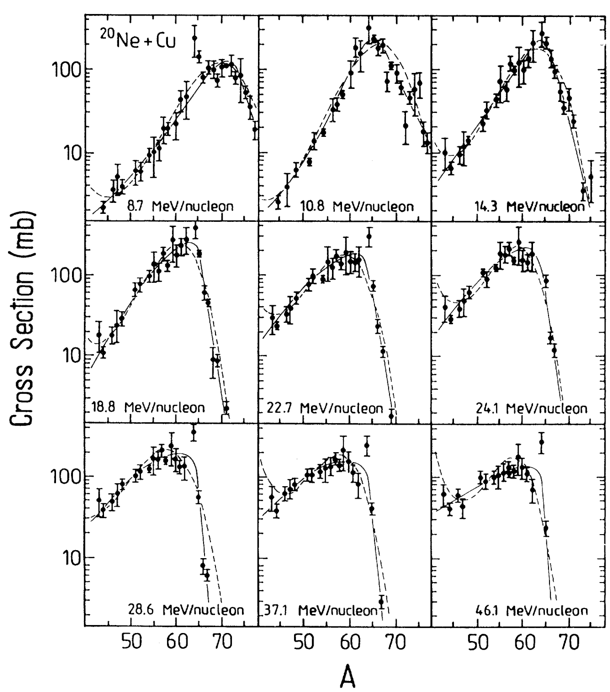

FIG. 4. Mass yields for the production of heavy fragments in ^{20}Ne+^{nat}Cu reactions deduced from the experimentally determined cross sections of the radioactive products. The lines represent the cross section obtained with the help of Eq. (5) and with parameters deduced from a global fit with all experimental cross sections. Dashed line, Eq. (5a); continuous line, Eq. (5b).

tem, this nucleus can be reached by one-nucleon-transfer reaction from both target components ^{63}Cu and ^{65}Cu. Its cross section can be therefore substantially higher than for other nuclei.

B. Total heavy residue cross section

From the mass yields presented in Fig. 4, the heavy residue cross sections σ_{HR} were deduced. This was done by extrapolating the mass yields down to $A=20$ and summing the cross section from $A=20$ up to the highest mass observed for a given bombarding energy. In the extrapolation to the lower masses, an exponential drop of the mass yield was assumed in analogy to the high-energy reactions.[17] The cutoff of the mass distribution at $A=20$ reflects our concern to avoid the double counting, resulting from the cross section of the intermediate-mass fragments.[41] These fragments should have heavy partners, already included in the integration procedure.[9] The choice of the cutoff at $A=20$ is, evidently, somewhat arbitrary. However, the change in σ_{HR} when selecting this cutoff differently at, e.g., $A=30$ or 10, is negligible for all investigated energies but the three highest ones. For 46 MeV/nucleon this change is of 7% and 4% when using the cutoff at $A=30$ or 10, respectively. The cross sections of heavy reaction residues obtained by the integration of the exponential mass yield between $A=20$ and 42 amounts to 1%, 7%, and 25% of the σ_{HR} at 8.7, 22.7, and 46.1 MeV/nucleon beam energy, respectively.

Figure 5 presents, as a function of the projectile energy, the total cross section of the measured radioactive reaction products as well as the cross section obtained from the integration of the mass-yield distribution, as discussed above. The cross section of the radioactive reaction products amounts to about 800 mb and decreases slightly with the beam energy. This decrease can be due to the shift, with the increasing beam energy, of the mass distribution toward lighter-mass nuclei undetectable by the method used in this work (Fig. 4). The cross section obtained by the fitting and extrapolation procedure exceeds the cross section of the radioactive nuclei by about a factor of 2 at the lowest bombarding energies and by about a factor of 3 at the highest ones. On the average, the obtained cross section is about 15% lower than the reaction cross section σ_R calculated using the parametrization proposed by Kox *et al.*[42] However, at higher bombarding energies the agreement between the experiment and calculation is within the experimental errors.

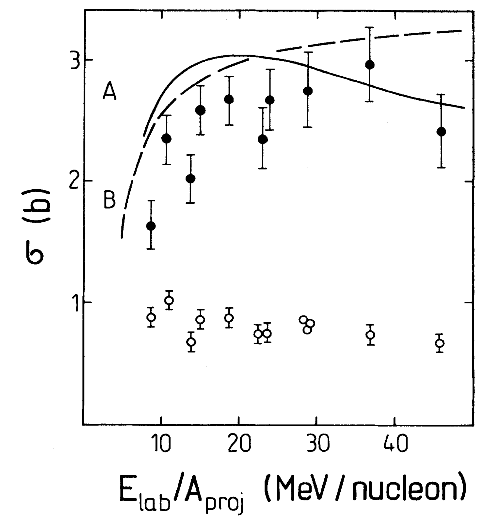

FIG. 5. Cross section of the reaction ^{20}Ne+^{nat}Cu as a function of the projectile energy per nucleon. Open circles represent the experimentally determined cross section of the radioactive reaction products. Solid circles represent heavy residue cross section σ_{HR} and are obtained through the integration of the mass yields (cf. Fig. 4) up to the product mass $A=20$. The curve A is the total reaction cross section σ_R calculated using the parametrization of Ref. 42 and curve B gives σ_R from Ref. 68.

C. Average and the most probable mass of the product

Another quantity which may be defined from the mass yield is the average cross-section-weighted mass of the heavy reaction product $\langle A_{prod} \rangle$. This average mass (calculated by including the cross sections obtained by extrapolation of the mass yields as described above) is presented in Fig. 6 as a function of the energy in the center-of-mass system $E_{c.m.}$, and is also given in Table IV.

Besides the ^{20}Ne+^{nat}Cu data, this figure also shows the average product mass for other heavy- and light-ion reactions on natural copper target. The ^{14}N data points below 400 MeV are from our work (see Introduction). Other data points are taken from the literature using, however, our fitting procedure (as described in Sec. III A) for consistency.

For the bombarding energies higher than about 200 MeV and within the existing experimental information, $\langle A_{prod} \rangle$ is almost identical for ^{12}C, ^{14}N, and ^{20}Ne reactions. For lighter projectiles (protons, ^{3}He, ^{4}He) and energies above about 500 MeV, this mass is slightly heavier—i.e., the average mass removed from the target,

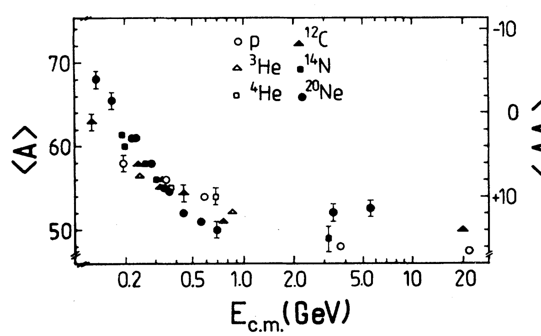

FIG. 6. Average mass of heavy product (left-hand scale) and average number of removed nucleons $\langle \Delta A \rangle = A_{target} - \langle A_{product} \rangle$ (right-hand scale) as a function of the c.m. energy for reactions with a ^{nat}Cu target. The proton data are from Refs. 17–19, the ^{3}He data from Ref. 20, the ^{4}He data from Ref. 16, the ^{12}C data from Refs. 9, 10, 28 and 31, the ^{14}N at 3.1 GeV from Ref. 17, the ^{20}Ne data above 1 GeV from Ref. 23, and the ^{14}N, ^{20}Ne data below 1 GeV from the present work.

TABLE IV. Summary of the experimental results. Numbers in parentheses represent uncertainties in the last significant digits.

Projectile	Beam energy (MeV/nucleon)	Cross section for heavy fragment production (b)	Reaction[a] cross section (b)	Average mass of the heavy product	Slope of the mass-yield curve (%)	Average velocity in v_{cn} units	Average[b] LMT $\langle p \rangle$ (GeV/c)	Maximum velocity in v_{cn} units	Maximum[b] LMT p_{max} (GeV/c)
^{20}Ne	8.7	1.60(20)	2.50	68.0(4)	16(3)	0.72(5)	1.70(12)	1.0(1)	2.56(26)
	10.8	2.35(20)	2.75	65.5(4)	23(3)	0.75(5)	1.96(11)	1.0(1)	2.82(26)
	14.3	2.00(20)	2.95	61.0(5)	19(3)	0.62(4)	1.80(12)	0.80(8)	2.40(25)
	15.0	2.55(20)	2.95	61.0(6)	22(3)	0.66(4)	1.99(12)	0.84(8)	2.69(25)
	18.8	2.65(20)	3.05	58.0(7)	18(3)	0.57(3)	1.87(12)	0.75(7)	2.62(24)
	22.7	2.35(25)	3.00	55.0(8)	13(2)	0.48(3)	1.69(12)	0.63(6)	2.29(23)
	24.1	2.65(25)	3.00	54.5(8)	12(2)	0.51(4)	1.86(13)	0.67(6)	2.55(23)
	29[c]	2.75(30)	2.95	52.0(10)	9.0(15)	0.43(3)	1.69(13)	0.56(6)	2.26(23)
	37.1	2.95(30)	2.80	51.0(10)	8.0(10)	0.35(3)	1.51(17)	0.44(5)	1.96(22)
	46.1	2.40(30)	2.65	50.0(15)	7.5(10)	0.27(3)	1.32(15)	0.39(4)	1.94(22)
^{14}N	16.2	1.90(20)	2.70	61.5(4)	25(4)	0.72(5)	1.62(11)	0.9(1)	2.09(17)
	17.0	2.35(20)	2.75	60.0(4)	23(4)	0.68(5)	1.58(11)	0.9(1)	2.22(18)
	22.1	2.25(20)	2.70	58.0(5)	21(3)	0.58(4)	1.43(11)	0.71(8)	1.91(18)
	26.6	2.30(25)	2.65	56.0(5)	15(3)	0.50(4)	1.40(11)	0.61(8)	1.76(17)

[a]Reaction cross section is calculated using the parametrization proposed in Ref. 42.
[b]The primary recoiling mass was assumed to be $A = A_{target} + A_{transfer}$, and $A_{transfer}$ was obtained from the incomplete fusion model.
[c]The result quoted are the average values from the data obtained at 28.6, 28.7, and 29.2 MeV/nucleon beam energy.

$\langle \Delta A \rangle = A_{target} - \langle A_{prod} \rangle$, is slightly lower (compare the right axis in Fig. 6) than for heavy ions.

For heavy ions the average product mass decreases rapidly with the beam energy at a rate of 3.3 mass units per 100 MeV c.m. energy up to about 400–500 MeV beam energy. At this energy the rate of decrease of $\langle A_{prod} \rangle$ is rather abruptly slowed down. The $\langle A_{prod} \rangle$ for light projectiles seems to decrease more smoothly with the increasing energy. At high bombarding energies its value is, however, very similar to the average product mass observed with heavy ions.

For the ^{20}Ne+^{nat}Cu reaction, if one neglects the abnormal cross section of the mass 64, the most probable mass decreases from a value of $A_{MP} = 70 \pm 2$ at projectile energy of 8.7 MeV/nucleon up to the value of $A_{MP} = 59 \pm 2$ at 22.7 MeV/nucleon and remains constant thereafter, i.e., above 350 MeV energy in the center-of-mass system. Again, for a given c.m. energy the most probable mass is very similar for other heavy- and light-ion-induced reactions on the ^{nat}Cu target (see Ref. 43 for corresponding figure).

D. Slope of the mass-yield distribution

We have determined the logarithmic slope S of the mass-yield curve for product masses lighter than A_{MP}. This was done by fitting a simple exponential function to the part of the cross sections which, in the representation of Fig. 4, take the form of a straight line. Results are given in Table IV and are presented in Fig. 7 as a function of energy in the c.m. system. Similarly, we have done such a fit for other light- and heavy-ion-induced reactions with a natural copper target.

For a distribution characterized by a sharp drop of the cross sections for masses heavier than the target mass, the reciprocal of the average removed mass $\langle \Delta A \rangle^{-1}$ should be approximately equal to the logarithmic slope S. As can be verified with the help of the data presented in Table IV, this is, indeed, the case for distributions gathered at the highest bombarding energies.

The logarithmic slope of the mass-yield distribution attracted much attention in previous investigations of spallation reactions with a natural Cu target. Already in the original Rudstam paper,[15] dealing with light projectiles, the dependence of this slope on the particle and target mass was studied. It was found that the slope decreases rapidly with the beam energy up to a value of about $0.05 A^{-1}$ and stabilizes thereafter. The "turning point" between the decrease and stabilization of the slope was

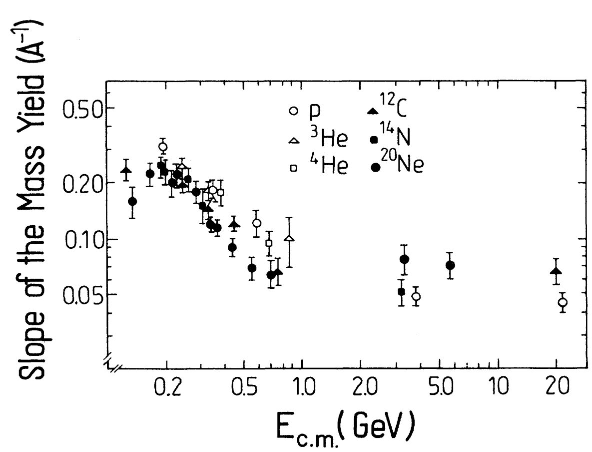

FIG. 7. Logarithmic slope of the mass yield as a function of the c.m. energy for reactions with the ^{nat}Cu target. See the caption of Fig. 6 for the data source.

found somewhere between 2 and 3 GeV bombarding energy.

Later Cumming *et al.*[4] presented a systematic study of the mass-yield slope as a function of the projectile kinetic energy in the laboratory reference frame for light ions from 200 MeV up to 30 GeV and heavy ions for GeV energies. The slope was correlated with the excitation energy transferred from the bombarding particle: A smaller slope corresponds to higher average deposited energy and vice versa. The "stabilization" of the slope observed by Rudstam at a level around $0.05A^{-1}$, at energies above 2–3 GeV, was confirmed for light, but also for heavy, ions.

More recently, Campi, Desbois, and Lipparini,[5] using the relation between mass-yield slope and average removed mass, estimated the limit value of the average deposited energy. This value was found to be about 3 MeV/nucleon, independently of the target and projectile. Abul-Magd, Friedman, and Hufner[44] were able to derive the shape of the mass-yield curve for proton-induced reactions starting from "first principles," i.e., from the multiple scattering and an approximation to the evaporation chain. Finally, Gross *et al.*[45] discussed mass-yield distribution in proton- and heavy-ion-induced reactions using a model treating explicitly the target fragmentation process.

One of the results of the systematics of Cumming *et al.*[4] was a similarity of the mass-yield distribution for a given projecile energy for light and heavy projectiles. As the slope is a measure of the deposited energy, it was concluded that the deposited energy is governed solely by the projectile kinetic energy and not its mass.

In the systematics of Cumming *et al* the heavy-ion data were available only for bombarding energies above 3 GeV, where the mass-yield slope already saturates. Besides proton data, the only points available in the energy region where the slope is strongly dependent on the bombarding energy were the ^{4}He data. At present the slope systematics may be substantially extended in the intermediate-energy region (below 1 GeV) due to this work as well as some other data in the literature (see references to Fig. 6).

E. Velocities of the recoil nuclei

The observable of principal interest in the studies of nuclear reactions induced by light and heavy ions is the recoil velocity of heavy reaction residues acquired during the first, fast reaction stage. In the thick-target–thick-catcher experiment as performed in the present work, one attempts to determine the projection of this velocity on the beam axis by measuring the quantities FW and F/B previously defined in Sec. III. Generally, the problem is complicated due to the evaporation process which introduces a distribution to the primary recoil velocities. Because of this distribution, the FW product is different from the penetration depth even for a linear relationship between velocities and ranges. The problem complicates even more due to the nonlinearity in this relationship.

The methods of extracting the primary, parallel velocity of heavy reaction products form the thick-target–thick-catcher experiment have been discussed for decades.[13,46,47] They were recently summarized[9] for a particlar situation when the forward velocity imparted to heavy recoils is substantially larger than its evaporation width. Such a situation may be detected by a very large ratio of the forward-to-backward recoils ($F/B>100$). It is characteristic for the energetic heavy-ion reactions[9,30,31,39] as investigated in the present work.

For the ratio $F/B \geq 80$ as observed in our data the FW product would be equal to the penetration depth in case of linear range-velocity relationship. It may be shown (see Ref. 43 and Appendix) that for the real, nonlinear relationship between these quantities the FW values are still larger by a few percent than the penetration depth. This effect is, however, approximately compensated if for the range-velocity conversion one uses tables in which the integrated path length[48] instead of the penetration depth[49] is listed. Therefore, contrary to the procedure discussed in Ref. 9, using the Northcliffe-Schilling tables for the range-velocity conversion, we did not convert the tabulated path length to the projected ranges. Apparently, a similar approach was also adopted by others.[30]

Evidently, we do not claim that the accidental compensation mentioned above is valid in other mass regions. In the region of interest here, this assumption is supported by the study of the ^{4}He- and ^{3}He-induced reactions on ^{59}Co using the thick-target–thick-catcher method.[7] In this study the backward recoils were also very small and the recoil velocities were calculated directly from the FW product using Northcliffe-Schilling tables. At bombarding energies below about 20 MeV/nucleon and for products much lighter than the target, these velocities were found, as expected, equal to the compound nucleus velocity. This result was recently confirmed by a thin-target–thin-catcher experiment.[14]

Another factor which should be considered when extracting the recoil velocities from the thick-target experiment is the change of the production cross section all along the target depth.[50,51] This effect can be of great importance when one investigates nuclear reactions induced by heavy ions of rather low bombarding energy. In the present work the worst still analyzable case was the ^{69}Ge nucleus produced using a 15.0-MeV/nucleon beam incident on a 14.7-mg/cm^2 target. It was estimated that in this case FW exceeds the range R by no more than 20%. For the products with mass numbers $A=43$–65, this discepancy is within 1%. FW cannot, however, be treated as an estimate of R for the products having $A>75$, and it is not possible to quantitatively evaluate the correction factor. Further analysis has not been, therefore, carried out for this mass range.

The recoil velocities gathered in the present work are shown in Fig. 8. Their numerical values are presented in tabular form in Ref. 43. The indicated errors are only statistical and, in particular, do not include the systematic errors resulting from the conversion of the measured FW values to the recoil ranges. The possible uncertainties[52] in the tabulated range-energy values[48] are also neglected.

In Table IV, for each bombarding energy, the average recoil velocity is listed. We determine this velocity by

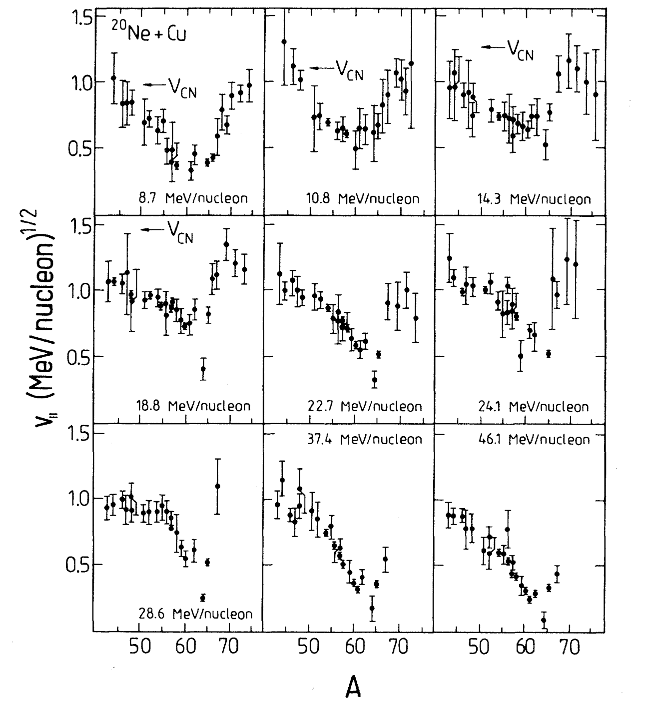

FIG. 8. Recoil velocity of heavy products as a function of the product mass for $^{20}Ne+^{nat}Cu$ reaction. The arrows indicate the recoil velocity expected for a reaction product formed by complete fusion of the target and projectile.

folding together, for each bombarding energy, the mass and velocity distributions presented in Figs. 4 and 8. The mass distribution is extrapolated to lower masses as discussed in Sec. IV B. It is assumed that in this distribution the light, unobserved products have velocity corresponding to the velocity of the lightest observed radioactive products (plateau region; see below).

In our previous works[7,8,14,53] we have observed that in light- and heavy-ion-induced reactions the recoil velocities "saturate" for products lighter and far removed from the target, and that a "plateau" of these velocities is formed. Such a plateau was also observed by others[9,30,31] and may be discerned in almost all velocity distributions presented in Fig. 8. We identify the velocities of this plateau as the maximum velocity, which may be acquired during the interaction of a given projectile and target nucleus at a given bombarding energy. This definition excludes the reaction products heavier than the target mass and observed with a small cross section at, e.g., 18.8 MeV/nucleon (see Fig. 8). In our defnition we also exclude very light nuclei of mass $A \leq 24$, observed, e.g., in Refs. 9 and 30. These nuclei are most probably of a quite different nature with different kinetic properties[41] than the target residues considered here.

For the light-ion (^3He,^4He)-induced reactions in this mass region,[8] the cross section corresponding to the reaction products with the plateau velocity is rather small (of the order of 100 mb). Therefore, for these reactions it was reasonable to assume[7] that the products exhibiting the plateau velocity originate from central collisions, characterized by a complete overlap between projectile and target.[54] This is not the case for heavy ions (^{12}C, ^{14}N, ^{20}Ne) interacting with a Cu target. For bombarding energies between 20 and 46 MeV/nucleon, the cross section corresponding to the plateau region is in these reactions of the order of 1100 mb (±200 mb). This corresponds approximately to the range of impact parameters from zero to the target radius. It can be shown[43] that the "fusionlike collisions" observed in heavy-ion reactions with fissionable targets[55] correspond approximately to the same range of impact parameters.

In the recoil velocity data from heavy-ion-induced reactions measured in the present work, as well as in other similar investigations, no clear signature of the complete overlap collisions can be discerned, in agreement with the discussion of the radial density distribution in nuclei presented in Ref. 22. Therefore, in the following we will identify as central collisions all these interactions in which the heavy reaction product exhibits the plateau velocity. The recoil velocity of central collisions defined this way is given in Table IV and is presented in Fig. 9 as a function of the projectile E/A ratio for the $^{20}Ne+^{nat}Cu$ reaction. In this figure the results obtained from some reaction models are also shown. They are discussed in Sec. V.

F. Primary mass of the recoil nuclei

As seen in the previous section, the recoil velocity of heavy reaction residues acquired after the first, fast reac-

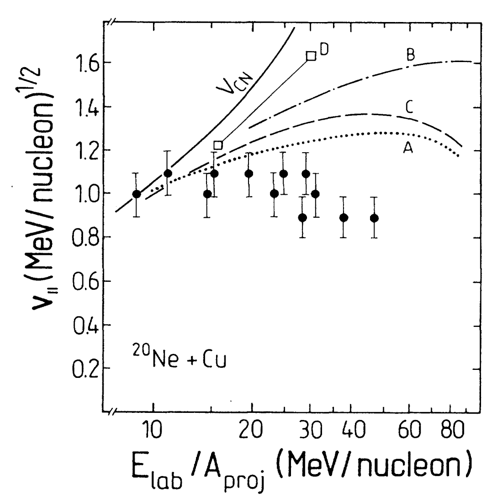

FIG. 9. Recoil velocity of heavy reaction residues produced in central collisions during the ^{20}Ne interaction with the ^{nat}Cu target as a function of the projectile energy per nucleon. The thick continuous line shows the recoil velocity expected for a reaction product formed by complete fusion of the target and projectile. The recoil velocity after central collisions as predicted by some models is also shown: Curve A gives the recoil velocity in a simple Fermi sphere approach (Ref. 82); curve B is obtained using the model of Ref. 83; curve C is calculated using Boltzmann master equation model (Ref. 64); curve D connects the results of Landau-Vlasov calculation at two energies (represented by open squares) as discussed in Sec. V D.

tion stage could be deduced from the thick-target–thick-catcher experiment. In principle, in order to be able to discuss other properties of these residues, their mass (before the evaporation process) should also be known. This mass can be obtained from observed velocities only under the assumption of a particular reaction model. A commonly used model[56,57] pictures the interaction of a lighter projectile with a heavier target as an extreme incomplete fusion process. In this process the part of the projectile interacting with the target, A_{transfer}, is captured forming a prefragment of the mass $A_{\mathrm{PF}} = A_{\mathrm{target}} + A_{\mathrm{transfer}}$. The remaining part of the projectile $N_{\mathrm{PE}} = A_{\mathrm{projectile}} - A_{\mathrm{transfer}}$ escapes (as a whole, as clusters, or as individual nucleons) with the beam velocity at zero degrees. Although this crude reaction model is certainly an oversimplification,[58] we will use it, following others, to estimate from our mass and velocity data the linear momentum transfer (LMT) and the prefragment excitation energy. In discussing the obtained results, we shall, however, remember the assumption made. Figure 10 presents as a function of ^{20}Ne energy per nucleon the average and maximum (for the plateau velocity) values of the prefragment mass A_{PF}. For central collisions we assume here also that the decrease of the recoil velocity below that corresponding to the compound nucleus is due to the emission of fast nucleons having the beam velocity on the average[59] and emitted at zero degrees.[60]

G. Average linear momentum transfer

The average linear momentum transfer from the projectile to the heavy reaction residues is obtained by multiplying the average recoil velocity by the average mass of the prefragment, or by folding together the mass and velocity distributions. The difference between the average LMT obtained by these two approaches is below 2% for all bombarding energies in this work. The average (LMT) obtained by the first approach is given in Table IV and is shown in Fig. 11.

We have previously presented[32] the systematics of the average linear momentum transfer in light- and heavy-ion-induced reactions in the mass region around $A = 60$. At that time we calculated the average LMT from the recoil velocity of the radioactive nuclei only. These nuclei were considered as a statistical sample[7] of the whole population of heavy reaction products. After the evaluation of the mass distributions in the ^{20}Ne+$^{\mathrm{nat}}$Cu reaction, we realized that this approximation may not be adequate for the highest bombarding energies investigated in this work. At these energies an important part of the heavy product cross section goes to nuclei with mass lower than 43, which went undetected in our work. Therefore, for these energies the radioactive nuclei cannot be considered as an unbiased sample.

At the highest ^{20}Ne bombarding energy, the present average LMT value is about 10% higher than previously found.[32] This difference, however, does not change the conclusions from our previous work. In particular, the present systematics confirms the suggestion of Ref. 32 concerning the projectile dependence of LMT. It is seen in Fig. 11 that at a given beam velocity the average LMT divided by the projectile mass decreases with the increase of this mass, at least up to projectiles as heavy as ^{20}Ne. This effect was not observed for heavy, fissile targets[61] for which, at a given $E/A_{\mathrm{projectile}}$, the average LMT per projectile nucleons is the same for all ions with mass equal or heavier than 12.

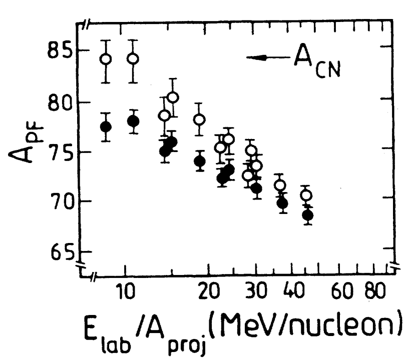

FIG. 10. Calculated mass of the prefragment A_{PF} after the fast reaction step and before the evaporation process as a function of the projectile energy per nucleon for the ^{20}Ne+$^{\mathrm{nat}}$Cu reaction. The mass of the prefragment is obtained under the assumption that beam velocity nucleons (or clusters) emitted at zero degrees account for the experimentally observed recoil velocity. Solid circles correspond to the average prefragment mass and open circles to the prefragment in central collisions. The arrow indicates the mass of the product formed by complete fusion of the target and projectile.

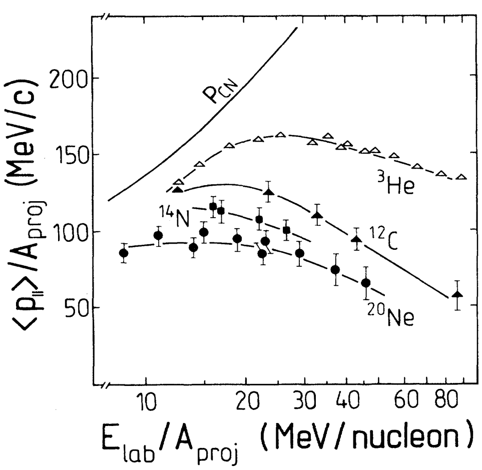

FIG. 11. Average linear momentum transfer (LMT) divided by A_{proj}, the mass of the projectile, as a function of the bombarding energy divided by A_{proj} for ^{12}C, ^{14}N, and ^{20}Ne ions interacting with the $^{\mathrm{nat}}$Cu target and for ^{3}He ions interacting with the ^{59}Co target. The ^{3}He data are from Ref. 32, the ^{12}C points are calculated from the data of Refs. 31 and 29, and the ^{14}N, ^{20}Ne data are from the present work. The thick continuous line gives the beam momentum or the momentum of a product formed by complete fusion of the target and projectile. Other lines are to guide the eye. See also Fig. 10 concerning the assumed value of the recoiling mass.

H. Linear momentum transfer for central collisions

Similarly as the average LMT, the maximum LMT, corresponding to central collisions as defined in Sec. IV E, is obtained by multiplying the maximum velocity (given in Table IV in compound nucleus velocity units) by the mass of the recoiling prefragment. This mass is again calculated assuming the incomplete fusion mechanism for reactions leading to heavy fragments with the plateau velocity. The values of the maximum LMT are presented in Table IV.

I. Average excitation energy of primary reaction products

As discussed in Refs. 7 and 31, there are two approaches for the determination of the average excitation energy from the mass and velocity distribution gathered in the studies presented here or in similar investigations. Both these approaches rely to a different degree on the assumption of the incomplete fusion model, discussed in Sec. IV F.

The first approach[62,63] is based solely on the kinematic properties of heavy recoils and, using the incomplete fusion assumption, gives the average excitation energy in the form

$$\langle E^* \rangle = \tfrac{1}{2} v_{\mathrm{recoil}} v_{\mathrm{beam}} A_{\mathrm{target}} + Q \ , \tag{10}$$

where v_{recoil} is the average recoil velocity as discussed in Sec. IV E and the last term represents the mass balance of the reaction. To calculate the reaction Q value, it was often assumed[31,57] that the missing mass escapes as free nucleons. The solid circles in Fig. 12 represent the average excitation energy calculated from the formula (10) under this assumption. The data for ^{12}C, ^{14}N, and ^{20}Ne projectiles are shown there as a function of the center-of-mass energy.

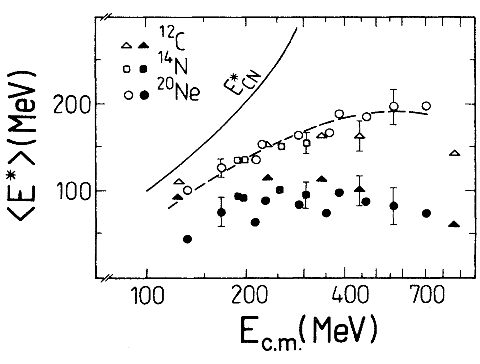

FIG. 12. Average excitation energy of the equilibrated, hot system after the interaction of ^{12}C, ^{14}N, and ^{20}Ne projectiles with the ^{nat}Cu target as a function of the c.m. energy. The ^{12}C points are calculated from the data of Refs. 9 and 29–31; ^{14}N, ^{20}Ne points are from the present work. The incomplete fusion reaction mechanism is assumed in the extraction of $\langle E^* \rangle$ from the experimental data. The solid circles are obtained using only the kinematic properties of heavy reaction residues (Ref. 62) and the assumption that the missing mass escapes as free nucleons. Open circles are obtained in the same way, but assuming the Q value in Eq. (10) equal to zero. The thick continuous line represent the excitation energy of the complete fusion product. The dashed line gives the average excitation energy calculated using the average number of nucleons evaporated from the prefragment (see also text).

Open circles in this figure are obtained under the assumption that the reaction Q value is equal to zero. This approximately corresponds to the situation in which the missing mass is emitted in the form of one nonexcited cluster. In view of the abundant emission of the intermediate-mass fragments in heavy-ion collisions at intermediate energies,[41] this possibility cannot be ignored. Therefore, we conclude that the average excitation energy obtained from the kinematic properties of heavy recoils under the assumption of the incomplete fusion reaction mechanism is contained somewhere between solid and open circles in Fig. 12.

In another approach,[5,7] in order to estimate the average excitation energy, one uses an independent observable, the experimentally determined average number of nucleons evaporated from the prefragment and the mean excitation energy necessary to evaporate a single mass unit. The product of these two quantities would be equal to the average excitation energy. The problem is that the experiment determines the average number of nucleons removed from the target and the mass of the prefragment is unknown. Campi, Desbois, and Lipparini[5] assume this mass to be equal to the target mass. On the other hand, in Refs. 7 and 31 the prefragment mass was obtained from the incomplete fusion assumption as discussed in Sec. IV F. The adoption of the last assumption makes both approaches in some way interrelated.

The dashed line in Fig. 12 represents the average excitation energy obtained using the second approach for the $^{20}Ne+^{nat}Cu$ reaction. The mean excitation energy necessary to evaporate a single mass unit, $\langle e \rangle$ (assumed to be independent of the excitation energy and equal to 10 MeV/nucleon), was obtained from the evaporation calculation as discussed in Sec. V. As can be seen, the second approach agrees only with the upper limit of the first one. A similar effect was already signalized for ^{12}C projectile interacting with a ^{nat}Cu target.[31] Here it is confirmed for other projectiles.

The data of Figs. 12 and 10 indicate that in the interaction of ^{12}C, ^{14}N, and ^{20}Ne ions with the ^{nat}Cu target, the average excitation energy does not exceed 3 MeV/nucleon.

J. Excitation energy for central collisions

We assume that the excitation energy for central collisions is correlated with the maximum recoil velocity of heavy reaction residues. In order to calculate this energy, we again use formula (10), replacing v_{recoil} by $v_{\mathrm{recoil}}^{\mathrm{max}}$ (see Table IV, column 9) and assuming this time that the missing mass is emitted in the form of individual nucleons.[59,64] The excitation energy per nucleon $\varepsilon^*_{\mathrm{central}}$ of the prefragment formed in $^{20}Ne+^{nat}Cu$ central collisions calculated under these assumptions is shown in Fig. 13 as a function of projectile energy per nucleon. This figure also compares the experimental data with model calculations, which are discussed in the following section.

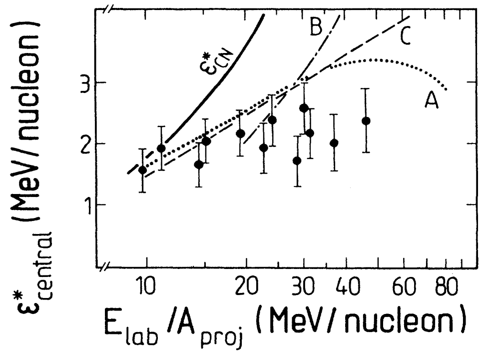

FIG. 13. Excitation energy per nucleon reached in central collision of ^{20}Ne with the ^{nat}Cu target. The missing mass escaping as free nucleons is assumed. Curves A,B,C give the excitation energy calculated using the same reaction models as in Fig. 9. The curve denoted ε^*_{CN} represents the excitation energy per nucleon in complete fusion of the target and projectile.

The absolute maximum of the excitation energy is attained for the bombarding energy at which the lightest reaction products are still formed by the complete fusion process. At higher bombarding energies the emission of preequilibrium nucleons makes this energy saturate.

A similar calculation of $\varepsilon^*_{central}$ performed for ^{12}C and ^{14}N ions interacting with a ^{nat}Cu target indicates that for a given center-of-mass energy, within errors, there is no difference between $\varepsilon^*_{central}$ for ^{12}C, ^{14}N and ^{20}Ne projectiles.

V. DISCUSSION

A. Mass and recoil velocity distributions

The heavy product mass yields can result from a number of processes. During the fast step of the reaction, the hot prefragment is produced, being a remnant of the fusionlike process, of a quasielastic or deep-inelastic process, or, for higher energies, of a target abrasion or target fragmentation process. After reaching thermodynamic equilibrium the prefragment evaporates light particles or undergoes a binary decay, and the experimentally observed mass distribution results.

The relative contribution of the above-mentioned processes to the observed mass distribution may be difficult, if not impossible, to untangle from an inclusive experiment as reported here. Therefore, without pretending to present a complete explanation of the observed mass-yield distribution, we shall in this section point out some systematic trends and compare our results with relevant data from the literature. In the effort to understand the observed mass distribution, at least qualitatively, we shall take advantage of the velocity distribution gathered in this work.

As can be seen from Fig. 4, the mass distributions of the heavy reaction products change their shape with increasing beam energy. For energies below 15 MeV/nucleon the mass distributions are almost symmetric, while for energies above 30 MeV/nucleon strongly asymmetric shapes are observed. The average and most probable mass of the product decreases smoothly with beam energy (Fig. 6). The same is true for the logarithmic slope of the mass yield (Fig. 7). At bombarding energies above 200 MeV, all these observables are almost identical for heavy ions as different as ^{12}C and ^{20}Ne and not too different from the average product mass and logarithmic slope observed with light projectiles. At low bombarding energies of about 10 MeV/nucleon, a somewhat surprising result is the observation, with a noticeable cross section, of nuclei with mass number as low as 44. As the velocities of these nuclei are close to the compound-nucleus velocity (see Fig. 8), they presumably result from the evaporation process following the complete fusion of the target and projectile. Therefore, the evaporative mass loss is there of about 40 nucleons with an excitation energy around 200 MeV. Such a large mass loss cannot be explained by the light-particle evaporation process alone.

Even before discussing the result of our evaporation calculations, it may be conjectured from previously published results[65–67] that the evaporation of heavy clusters (or, in other words, the compound-nucleus binary decay) can probably account for the important cross section observed for the lightest heavy fragments.

Indeed, our system of ^{20}Ne+^{64}Cu has the critical angular momentum for complete fusion reaction, l_{cr}, equal[68] to 55$\hbar$. This value is between l_{cr} of ^{63}Cu+^{12}C ($l_{cr}\approx 39\hbar$) and ^{63}Cu+^{27}Al ($l_{cr}\approx 71\hbar$) studied in Ref. 65. In that reference the cross section of products removed about 40 mass units from the compound nucleus was about 1 and 50 mb for 136 MeV c.m. energy ^{63}Cu+^{12}C and 238 MeV c.m. energy ^{63}Cu+^{27}Al, respectively. For about 200 MeV c.m. energy ^{20}Ne+^{nat}Cu, the cross section of products in this mass region is closer to 1 rather than 50 mb. This may be due to the fact that both for ^{63}Cu+^{12}C and ^{20}Ne+^{nat}Cu reactions the critical angular momentum for compound-nucleus formation is below the Businaro-Galone point (found in Ref. 65 to be equal to about 60$\hbar$) and for ^{63}Cu+^{27}Al above. An evaporation code, which besides treating light fragment evaporation in a conventional way, allows compound nuclei to decay by complex-fragment emission, was able to reproduce the cross sections of ^{12}C-induced reactions fully and the cross sections of ^{27}Al-induced reactions within a factor of 2–3.

When the lightest observed masses at bombarding energies of about 10 MeV/nucleon exhibit the recoil velocities close to the ones expected for the full momentum transfer, the slightly heavier products already recoil noticeably more slowly (see Fig. 8). The minimum recoil velocities (minimum LMT) are observed for the products close to the target. For the transtarget nuclei the LMT increases again and reaches the value of the full momentum transfer for the heaviest observed products. The V-shaped distribution of the recoil velocities centered around the target should reflect a strong contribution of the inelastic collisions to the cross section of the close-to-the-target products. As can be seen from Fig. 8, the V shape is slightly asymmetric, with steeper slope on the heavier-mass side. It is in agreement with the supposed inelastic contribution at around 10 MeV/nucleon bombarding energy. After the transfer of a few nucleons *to* the target, the evaporation process brings the final mass again close to the target mass. After the pickup of a few nucleons *from* the target, the evaporation additionally moves the final product mass away from the target. This process is superimposed on the light-particle and heavy-fragment emission from the compound system recoiling with the full transferred momentum. As a result, the left branch of the V-shaped distribution is less steep. If this description of the reaction mechanism around 10 MeV/nucleon is correct, the recoil velocities of the products around the target mass should have two components, one very small, corresponding to the inelastic reactions, and another one corresponding to the full momentum transfer. Evidently, the thick-target experiment gives for these nuclei only an average recoil velocity, weighted by a relative contribution of these two processes to the product cross section. As yet, no thin-target–thin-catcher results are available for the investigated reaction around 10 MeV/nucleon to check this hypothesis. However, the differential recoil ranges measured by Parker *et al.*[69] in a similar reaction at comparable energy per nucleon support the assumption of a two-component velocity distribution for the products close to the target.

For the bombarding energies around 14–18 MeV/nucleon, the most important channel of the fusion-evaporation process, the light-particle emission, reaches the final products having masses around the target mass. As a result, the component with higher momentum transfer in the recoil velocity for these products dominates and their average velocities are substantially more significant than at 8.7 MeV/nucleon bombarding energy.

At these energies the velocity distributions signal the appearance of a new reaction mechanism. Even for the lightest observed products, these velocities are below the compound-nucleus velocity: Fusion becomes less complete, even for the most central collisions. The mechanism which makes the fusion less complete and removes the linear momentum can be the onset of preequilibrium nucleon emission,[70] nonequilibrium emission of the intermediate-mass fragments,[41] or absorptive breakup of the projectile.[71] Although conceptually these processes are different, the experimental distinction between them is often difficult and, by the methods described here, impossible. Therefore, these mechanisms are only listed here. In the following section we will compare our recoil velocity results with model predictions to see if some reasonable interpretation can be proposed.

For even higher bombarding energies the cross section of the transtarget products becomes very small and almost disappears for the highest bombarding energies. At these energies the mass-yield distributions are already similar to the typical, strongly asymmetric spallation distributions observed for high-energy proton or heavy-ion-induced reactions.[17,18] In the velocity distribution the separation of peripheral and central collisions can still be discerned, although the main part of the plateau seems to move toward lighter masses, undetectable by our method.

B. Evaporation calculation

The distribution of the recoil velocities in Fig. 8 indicates that, even at the lowest bombarding energies employed in the present work, an important part of the heavy residue cross section originates from processes other than complete fusion. It cannot, therefore, be expected that the evaporation calculations reproduce the whole mass yields for these energies. They should, however, account for the lightest and heaviest masses observed at 8.7 and 10.8 MeV/nucleon bombarding energies which recoil with the compound-nucleus velocity. If these calculations do so, one may reasonably expect that they also correctly determine the mean excitation energy $\langle e \rangle$ necessary to remove a single mass unit, a quantity used to calculate the total excitation energy, as discussed in Sec. IV I.

The evaporation calculations were done for the beam energy around 10 MeV/nucleon and are compared with the experimental mass distribution in Fig. 14. Curve *A* represents the results of a calculation obtained with the ALICE program[72] with simple Ewing-Weisskopf approximation. The discrepancy between the calculated and experimental mass-yield curve is very large. Adding cluster evaporation into the ALICE program[73] changes the mass distribution, but not sufficiently to describe the cross section of the lightest products (curve *B*). In heavy-ion reactions a compound nucleus is produced with high angular momentum. This causes large deformation. The calculation with the full Hauser-Feshbach formalism, including deformation,[74] shows large cluster enhancement. Beckerman and Blann[75,76] showed that this effect can be simulated by a larger radius in the optical-model potential. Curve *C* represents the results of the evaporation calculation with cluster emission, but with radius 20% greater than the radius of the optical-model potential as calculated for a spherical nucleus. The agreement between experimental data and evaporation calculations is better, but the cross section of the lightest masses are still seriously

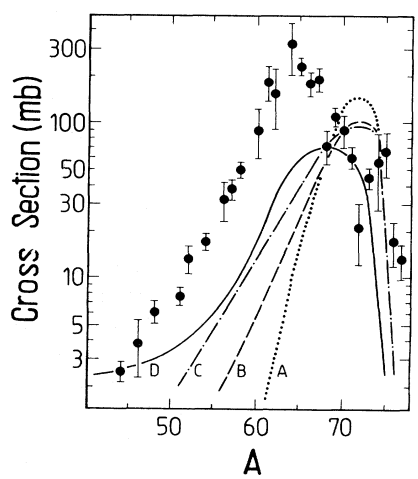

FIG. 14. Mass-yield distribution in a $^{20}Ne + ^{nat}Cu$ reaction at 10.8 MeV/nucleon bombarding energy compared with the evaporation calculations. Curve *A*: code ALICE (Ref. 72) and GEMINI (Ref. 77) and "classical" nucleon and α-particle emission; curve *B*: ALICE with an option allowing heavier cluster emission (Ref. 73); curve *C*: as curve *B*, but with optical potential well radius 20% greater than for spherical nucleus (see also text); curve *D*: GEMINI using option allowing cluster emission.

underestimated. Finally, curve *D* in Fig. 14 is obtained using the GEMINI code with an option allowing heavy cluster evaporation.[77] In this code the light-particle ($Z \leq 2$) evaporation probability is calculated using the Hauser-Feshbach formalism, with sharp cutoff approximation. For heavier fragments the probability of emission is calculated using the formalism proposed by Moretto,[78] with energy at the saddle point obtained from the Sierk model.[79] The last calculation is considered as describing fairly the cross section of the lightest and heaviest masses and was therefore used to calculate the $\langle e \rangle$ value. It was found that $\langle e \rangle$ depends little on the excitation energy and in the excitation energy range from 100 to 200 MeV is equal to 10.0 ± 0.5 MeV. This value is much smaller than that calculated in Ref. 44 for protons interacting with the ^{63}Cu target. The difference is due to the high angular momentum effects in ^{20}Ne reactions which strongly enhance heavy cluster emission. This in turn decreases the $\langle e \rangle$ value.

C. Comparison of experimental results for central collisions with model calculation

There exist at present a number of models which can predict the properties of heavy reaction residues issued from central target-projectile collisions. In Fig. 9 a comparison of the recoil velocities for nuclei in the "plateau" region (see Sec. IV E) with the predictions of some models is presented. Four models were considered. A simple Fermi sphere approach[80,81] was used in the way described in detail in Ref. 82. A model based on a two-body dissipation mechanism was used in the formulation presented in Ref. 83. Nuclear collision dynamics was taken into account in the model which semiclassically solves the Boltzmann master equation (BME model of Ref. 64). And finally the central and peripheral collisions recoil velocity was also compared wit the results of the Landau-Vlasov approach, presented in more details in the following section.

As can be seen from Fig. 9, at energies above 25 MeV/nucleon all considered models more or less overestimate the maximum velocity observed in the experiment. Although the reason for this discrepancy is not obvious, it can perhaps be attributed to the inclusion in the experimental central collisions of all collisions with impact parameter from zero to the target radius. On the other hand, the calculations are strictly applicable to collisions in which target and projectile overlap completely.

In Fig. 13 the comparison of the prefragment excitation energy in central collisions with the discussed models is presented. Similarly as the recoil velocity, the calculated excitation energy is more or less overestimated for bombarding energies above 30 MeV/nucleon. The reason for this discrepancy can be also due to the assumption made in the extraction of the excitation energy from the experimental data. In particular, good agreement between the experimental points and the calculation would be obtained if the mass balance in the fast reaction stage [Q in Eq. (10)] was assumed to be close to zero.

D. Simulation of the reaction solving Landau-Vlasov equation

After the comparison of our experimental data with central collision models, we have also attempted to calculate the reaction kinematics using a more sophisticated approach. This approach consisted in solving Landau-Vlasov (LV) equation for a few selected initial conditions. [We are using here the terminology employed, e.g., in Ref. 84. The LV equation is also denominated as Boltzmann-Uehling-Uhlenbeck (BUU) equation; see Ref. 85.] The GANIL version[86] of the solution procedure was employed. The ^{20}Ne+^{64}Cu collisions were simulated for the bombarding energies of 15 MeV/nucleon (impact parameters $b=0$ and 4 fm), 30 MeV/nucleon ($b=0$, 2, 4, and 6 fm), and 60 MeV/nucleon ($b=0$ and 4 fm). The details are presented in Ref. 43. The phase-space distribution of nucleons was investigated at time intervals of 40 fm/c between 0 and 280 fm/c. The thermalization time of the heaviest reaction product was determined observing the change of its mass (within a radius of 6.5 fm) as a function of time. For 15 and 30 MeV/nucleon this thermalization time was found to be somewhere between 150 and 200 fm/c and was identified through the stabilization of the heavy-fragment mass during some time interval. This stabilized mass was considered as the mass of a heavy prefragment at the end of the preequilibrium emission and before the evaporation process. Evidently, with the increasing bombarding energy, the separation of these two processes becomes more and more ambiguous.

The value of the recoiling mass and its recoil velocity as a function of the impact parameter are shown in Fig. 15 for the bombarding energy of 30 MeV/nucleon. The average, cross-section-weighted recoil velocity calculated from the data of Fig. 15 is 0.41 in compound-nucleus velocity units, v_{CN}, in perfect agreement with the experimental value of $0.43(3)v_{CN}$ (see Table IV). This agreement is, however, most probably fortuitous. In Fig. 9 it was already shown that at 30 MeV/nucleon bombarding

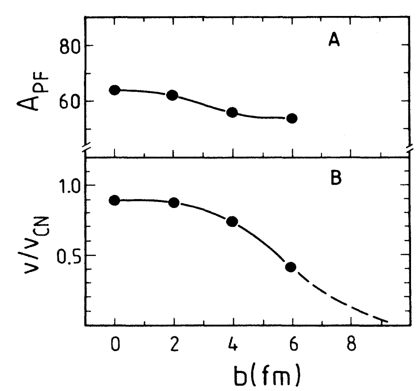

FIG. 15. Results of the Landau-Vlasov simulation for the ^{20}Ne+^{64}Cu reaction at 30 MeV/nucleon bombarding energy. (A) The mass of the heavy prefragment and (B) its recoil velocity in compound-nucleus velocity units are presented as a function of the impact parameter. The dashed line in (B) shows the assumed extrapolation of the recoil velocity on the impact parameters for which the calculations were not performed.

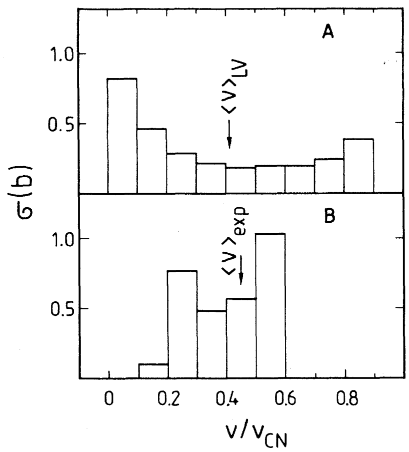

FIG. 16. Comparison of experimental and theoretical (Landau-Vlasov model) velocity distributions. The theoretical distribution is for the ^{20}Ne+^{64}Cu reaction at 30 MeV/nucleon. The experimental distribution is deduced from the thick-target results under the assumptions discussed in the text.

energy the LV calculation seriously overestimates the recoil velocity for central collisions. In Fig. 16 we compare the theoretical velocity distribution with the experimental distribution of the *average* recoil velocities of all heavy reaction products obtained using the present thick-target experiment. As can be seen, the theoretical and experimental distributions are quite different.

In preparing this figure it was assumed that the experimental average recoil velocities for each product mass are equal to the recoil velocity of the corresponding prefragment. A thin-target–thin-catcher experiment, not yet performed for the investigated reaction, could shed some light on this question.

A comparison between a BUU calculation and the experimentally determined recoil velocities was recently reported for other systems.[87] Similarly as in the present calculation, good agreement was obtained between the experiment and the BUU simulation for the recoil velocity integrated over all impact parameters. The maximum (or the most probable) recoil velocity was, however, seriously overestimated by the calculation, confirming the results of Figs. 9 and 16.

VI. SUMMARY AND CONCLUSIONS

In this work we have investigated the heavy reaction products issued from the interaction of ^{14}N and ^{20}Ne projectiles with a natural Cu target at a number of bombarding energies between 8 and 46 MeV/nucleon. The thick-target–thick-catcher recoil range technique has been used. The production cross section and the recoil velocity of the radioactive reaction residues have been determined. The quantities deduced from these experimental data were compared to other light- and heavy-ion results obtained using a similar technique and a natural Cu target.

Using a by now well-established minimization procedure, the charge dispersions and complete mass-yield distributions were deduced from the measured cross sections. The total cross section inferred from this procedure amounts to about 85% of the reaction cross section, calculated with the recently proposed parametrization. By folding the mass-yield distribution with the velocity distribution, the average linear momentum transfer (LMT) was obtained as a function of the projectile bombarding energy. At a given projectile velocity, the average LMT per projectile nucleon shows a dependence on the projectile mass for both light- and heavy-ion-induced reactions.

For reaction products that are lighter and far removed from the target, one observes a saturation of the recoil velocities as a functon of the mass removal. This saturation ("plateau") is a general phenomenon observed for light- and heavy-ion-induced reactions at intermediate energies and is interpreted as a manifestation of central collisions. The corresponding cross section for heavy ions indicates that the impact parameter of such defined central collisions is much larger than expected for complete overlap events and spans the range from zero up to the target radius. For ^{20}Ne+$^{\mathrm{nat}}$Cu reactions, the recoil velocity corresonding to these central collisions is equal to the compound-nucleus velocity up to about 11 MeV/nucleon bombarding energy and slowly decreases for higher energies.

The average excitation energy after the fast reaction step was deduced both from the kinematic properties of heavy recoils and from the average mass of the product. At a given center-of-mass energy, the average excitation energy is independent of the mass of the heavy ion for ^{12}C, ^{14}N, and ^{20}Ne projectiles. It strongly depends, however, on the assumptions of the mechanism of the fast reaction step. The collected data indicate that the average excitation energy of the prefragment attains its maximum value in the energy range below 1 GeV and that this maximum value does not exceed 3 MeV/nucleon.

Some of the experimental data gathered in the present work were compared with the predictions of reaction models. In our opinion the most interesting result of these comparisons is a strong indication that the Landau-Vlasov approach is unable to correctly describe the velocity distribution in the ^{20}Ne+$^{\mathrm{nat}}$Cu reaction.

ACKNOWLEDGMENTS

Our sincere thanks are due to Marshall Blann, Robert Charity, and Eric Suraud for providing us with their reaction mechanism codes and numerous discussions. Discussions with Joel Galin, Christian Grégoire, Eryk Infeld, Hans Plendl, and Wojciech Skulski are also highly appreciated. The help of Tadeusz Batsch and Iza Zychor in the data collection stage of this work and of Piotr Lubiński in some calculations is warmly acknowledged. This work was done within the IN2P3-Warsaw University Collaboration Agreement and was also supported by the Polish National Research Program CPBP 01.09.

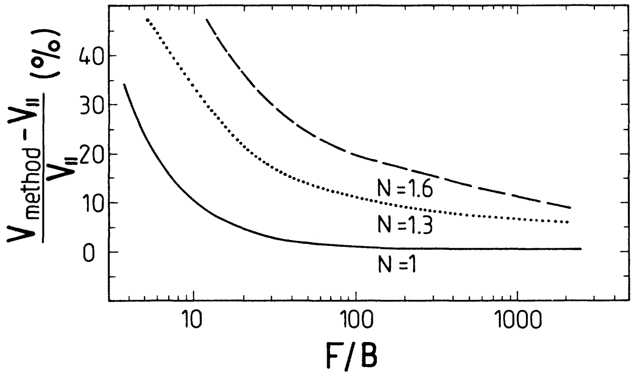

FIG. 17. Systematic error η of the velocity v_{method} vs the quantity F/B. Continuous line presents the results of the calculations for a linear dependence between range and velocity, $R=kV^N$, $N=1$. Dotted and dashed lines are for $N=1.3$ and 1.6, respectively.

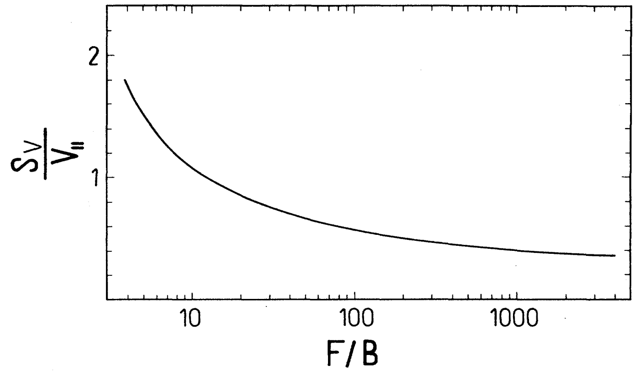

FIG. 18. Standard deviation of the velocity distribution S_v divided by the average recoil velocity $v_{\parallel}$ vs the quantity F/B.

APPENDIX: MONTE CARLO SIMULATION OF THE THICK-TARGET EXPERIMENT

Let us assume that the quantity FW, defined in Sec. III, is equal to the projected range R from which the velocity v_{method} is obtained. To estimate the systematic error introduced by this assumption, a Monte Carlo simulation of the experiment was performed with the following additional assumptions.

(a) The average velocity of the recoil nuclei, equal to $v_{\parallel}$, is parallel to the beam axis, and a distribution of velocities has a Gaussian shape with the standard deviation S_v.

(b) The relation between range and velocity can be parametrized by a commonly used formula $R=kV^N$, with N between 1 and 2.

(c) The target thickness is much greater than the width of the recoil range distribution.

(d) The cross section and the average recoil velocity is the same for reactions occurring at the front and back sides of the target.

We define the systematic error η of the calculated velocity v_{method} as $\eta=(v_{\text{method}}-v_{\parallel})/v_{\parallel}$. This error as a function of the ratio F/B (see Sec. III for definition) is shown in Fig. 17. It was found that the error η is very sensitive to the nonlinearity of the range-velocity relationship. For $F/B \gtrsim 100$ and $N \approx 1.3$ (the average N based on Northcliffe and Schilling tables), the v_{method} is greater than $v_{\parallel}$ by about 5–15 %.

For a linear dependence between the range and velocity ($N=1$), analytical relationships can be obtained for the error η, $S_v/v_{\parallel}$, and F/B ratio, using formulas given, e.g., in Ref. 13:

$$\eta=\frac{v_{\text{method}}-v_{\parallel}}{v_{\parallel}}=\frac{S_v}{v_{\parallel}}\frac{1}{\sqrt{2\pi}}\exp\left[-\left[\frac{1}{\sqrt{2}}\frac{S_v}{v_{\parallel}}\right]^2\right]-\frac{1}{2}\operatorname{erfc}\left[\frac{1}{\sqrt{2}}\frac{S_v}{v_{\parallel}}\right],$$

$$F/B=1+\frac{1}{\eta},$$

where erfc(x) is the error function defined as

$$\operatorname{erfc}(x)=\frac{2}{\sqrt{\pi}}\int_x^{\infty}\exp(-t^2)dt .$$

As expected, the result of the above analytical expressions for $N=1$, presented by a continuous line in Fig. 17, is the same as the result of the Monte Carlo simulation.

Finally, the ratio $S_v/v_{\parallel}$ vs F/B is shown in Fig. 18. Surprisingly, this ratio is almost independent on the nonlinearity in the relation between range and velocity for N between 1 and 2.

[1] J. Galin, H. Oeschler, S. Song, B. Borderie, M. F. Rivet, I. Forest, R. Bimbot, D. Gardes, B. Gatty, H. Guillemot, M. Lefort, B. Tamain, and X. Tarrago, Phys. Rev. Lett. **48**, 1787 (1982).

[2] M. B. Tsang, D. R. Klesch, C. B. Chitwood, D. J. Fields, C. K. Gelbke, W. G. Lynch, H. Utsunomiya, K. Kwiatkowski, V. E. Viola, and M. Fatyga, Phys. Lett. **134B**, 169 (1984).

[3] M. Fatyga, K. Kwiatkowski, V. E. Viola, C. B. Chitwood, J. D. Fields, C. K. Gelbke, W. G. Lynch, J. Pochadzalla, M. B. Tsang, and M. Blann, Phys. Rev. Lett. **55**, 1376 (1985).

[4] J. B. Cumming, P. E. Haustein, T. J. Ruth, and G. J. Virtes, Phys. Rev. C **17**, 1632 (1978).

[5] X. Campi, J. Desbois, and E. Lipparini, Nucl. Phys. **A428**, 327c (1984).

[6] J. Peter and B. Tamain, Grand Accélérateur National d'Ions, Lourds, Report No. Ganil P-87-24, 1987 (unpublished).

[7] J. Jastrzębski, P. P. Singh, T. Mróz, S. E. Vigdor, M. Fatyga, and H. J. Karwowski, Phys. Rev. C **34**, 60 (1986).

[8] J. Jatrzębski, in *Proceedings of the 5th International Conference on Nuclear Reaction Mechanism,* Varenna, 1988, edited by E. Gadioli (Ricerca Scientifica ed Educazione Permanente Suppl. 66, 1988), p. 175.

[9] S. Y. Cho, Y. H. Chung, N. T. Porile, and D. J. Morissey, Phys. Rev. C **36**, 2349 (1987).

[10]A. Lleres, J. Blachot, J. Crançon, A. Gizon, and H. Nifenecker, Z. Phys. A **312**, 177 (1983).
[11]E. Gadioli and P. E. Hodgson, Rep. Prog. Phys. **49**, 951 (1986).
[12]D. J. Parker, J. Asher, E. Gadioli, E. Gadioli-Erba, and J. J. Hogan, *Proceedings of the 5th International Conference on Nuclear Reaction Mechanism* (Ref. 8), p. 289.
[13]J. M. Alexander, in *Nuclear Chemistry,* edited by L. Yaffe (Academic, New York, 1968); Vol. 1, p. 273.
[14]W. Skulski, J. Jastrzębski, Q. Chen, M. Fatyga, and P. P. Singh, Phys. Rev. C **41**, 2605 (1990).
[15]G. Rudstam, Z. Naturforsch. **21a**, 1027 (1966).
[16]P. J. Karol, Phys. Rev. C **10**, 150 (1974).
[17]J. B. Cumming, P. E. Haustein, R. W. Stoenner, L. Mausner, and R. A. Naumann, Phys. Rev. C **10**, 739 (1974).
[18]J. B. Cumming, R. W. Stoenner, and P. E. Haustein, Phys. Rev. C **14**, 1554 (1976).
[19]C. J. Orth, B. J. Dropesky, R. A. Williams, G. C. Giesler, and J. Hudis, Phys. Rev. C **18**, 1426 (1978).
[20]E. Hagebø, I. R. Haldorsen, M. B. Mostue, J. Pettersen, O. Scheidimann, T. Lund, L. C. Caraz, and C. Richard-Serre, Radiochim. Acta **35**, 133 (1984).
[21]J. B. Cumming, P. E. Haustein, and H.-C. Hseuh, Phys. Rev. C **24**, 2162 (1981).
[22]G. D. Cole and N. T. Porile, Phys. Rev. C **24**, 2038 (1981).
[23]K. H. Hicks, T. E. Ward, M. Koike, and J. Peter, Phys. Rev. C **26**, 2016 (1982).
[24]G. D. Cole and N. T. Porile, Phys. Rev. C **25**, 244 (1982).
[25]P. E. Haustein and T. J. Ruth, Phys. Rev. C **18**, 2241 (1978).
[26]C. J. Orth, W. R. Daniels, B. J. Dropesky, R. A. Williams, G. C. Giesler, and J. N. Ginocchio, Phys. Rev. C **21**, 2524 (1980).
[27]S. Shibata, M. Imamura, T. Miyachi, M. Mutou, K. Sakamoto, Y. Hamajima, M. Soto, Y. Kubota, M. Yoshida, and I. Fujiwara, Phys. Rev. C **35**, 254 (1987).
[28]T. Lund, D. Molzahn, R. Brandt, B. Bergersen, D. Eriksen, E. Hagebø, I. R. Haldorsen, T. Bjørnstad, and C. Richard-Serre, Phys. Lett. **102B**, 239 (1981).
[29]T. Lund, D. Molzahn, B. Bergersen, E. Hagebø, I. R. Haldorsen, and C. Richard-Serre, Z. Phys. A **306**, 43 (1982).
[30]L. Kowalski, P. E. Haustein, and J. B. Cumming, Phys. Rev. Lett. **51**, 642 (1983).
[31]S. Y. Cho, N. T. Porile, and D. J. Morrissey, Phys. Rev. C **39**, 2227 (1989).
[32]T. Batsch, J. Blachot, Q. Chen, J. Crançon, M. Fatyga, A. Gizon, J. Jastrzębski, H. Karwowski, W. Kurcewicz, A. Lleres, T. Mróz, L. Pieńkowski, P. P. Singh, S. E. Vigdor, and I. Zychor, Phys. Lett. B **189**, 287 (1987).
[33]L. Pieńkowski, T. Batsch, J. Blachot, J. Crançon, A. Gizon, J. Jastrzębski, and W. Kurcewicz, in *Proceedings of the Third International Conference on Nucleus-Nucleus Collisions, Saint-Malo, June, 1988,* edited by C. Estève, D. Grégoire, G. Guerreau, and B. Tamain (Centre de Publications de l'Université de Caen, Caen, 1988), p. 63.
[34]G. Marguier, J. Giroux, A. Tabia, J. Blachot, J. Crançon, H. Nifenecker, and A. Gizon, Institut de Physique Nucleaire, Université Lyon, Rapport Annuel, 1984, p. 51.
[35]F. Hubert, A. Fleury, R. Bimbot, and D. Gardes, Ann. Phys. (Paris) Suppl. **5**, 1 (1980).
[36]H. P. Block, J. C. de Lange, and J. W. Schotman, Nucl. Instrum. Methods **128**, 545 (1975).
[37]V. B. Zlokazov, Nucl. Instrum. Methods **199**, 509 (1982); and W. Karczmarczyk, M. Kowalczyk, and L. Pieńkowski (unpublished).
[38]U. Reus and W. Westmeier, At. Data Nucl. Data Tables **29**, 2 (1983).
[39]J. B. Cumming (private communication).
[40]A. D'Onofrio, B. Delaunay, J. Delaunay, H. Dumont, J. Gomez del Campo, F. Andreozzi, A. Brondi, R. Moro, M. Romano, and F. Terrasi, Phys. Rev. C **35**, 1167 (1987).
[41]W. G. Lynch, Annu. Rev. Nucl. Part. Sci. **37**, 493 (1987).
[42]S. Kox, A. Gamp, C. Perrin, J. Arvieux, R. Bertholet, J. F. Bruandet, M. Buenerd, R. Cherkaoui, A. J. Cole, Y. El-Masri, N. Longequeue, J. Menet, F. Merchez, and J. B. Viano, Phys. Rev. C **35**, 1678 (1987).
[43]L. Pieńkowski, Ph.D. thesis, Warsaw University, 1991.
[44]A. Y. Abul-Magd, W. A. Friedman, and J. Hufner, Phys. Rev. C **34**, 113 (1986).
[45]D. H. E. Gross, L. Satpathy, Meng Ta-chung, and M. Satpathy, Z. Phys. A **309**, 41 (1982).
[46]N. Sugarman, M. Campos, and K. Wielgoz, Phys. Rev. **101**, 388 (1956).
[47]L. Winsberg, Nucl. Instrum. Methods **150**, 465 (1978).
[48]L. C. Northcliffe and R. F. Schilling, Nucl. Data Tables A **7**, 233 (1970).
[49]U. Littmark and J. F. Ziegler, *The Stopping and Ranges of Ions in Matter* (Pergamon, New York, 1977), Vol. 6.
[50]N. T. Porile, Phys. Rev. **127**, 224 (1962).
[51]H. Delagrange, A. Fleury, F. Hubert, and G. N. Simonoff, Phys. Lett. **37B**, 355 (1971).
[52]J. F. Ziegler and J. P. Biersack, in *The Stopping and Range of Ions in Matter, Treatise on Heavy-Ion Science,* edited by D. A. Bromley (Plenum, New York, 1985), Vol 6, p. 95.
[53]J. Jastrzębski, T. Batsch, J. Blachot, Q. Chen, J. Crançon, A. Gizon, W. Kurcewicz, L. Pieńkowki, and P. P. Singh, in Ref. 33, p. 64.
[54]G. Klotz-Engmann, H. Oeschler, J. Stroth, E. Kankeleit, Y. Cassagnou, M. Conjeaud, R. Dayras, S. Harar, R. Legrain, E. C. Pollacco, and C. Volant, Nucl. Phys. **A499**, 392 (1989).
[55]V. E. Viola, B. B. Back, K. L. Wolf, T. C. Awes, C. K. Gelbke, and H. Breuer, Phys. Rev. C **26**, 178 (1982).
[56]M. Lefort, J. Phys. (Paris) Colloq. **47**, C4-427 (1986).
[57]C. Leray, J. Phys. (Paris) Colloq. **47**, C4-275 (1986).
[58]E. Suraud, Ch. Grégoire, and B. Tamain, Prog. Part. Nucl. Phys. **23**, 357 (1989).
[59]J. P. Bondorf, J. N. De, G. Fai, and A. O. T. Karvinen, Nucl. Phys. **A333**, 285 (1980).
[60]G. Mantzouranis, H. A. Weidenmuller, and D. Agassi, Z. Phys. A **276**, 145 (1976).
[61]V. E. Viola, in Proceedings of the Symposium on the Many Facets of Heavy-Ion Fusion Reactions, Argonne, 1985, Argonne National Laboratory Report No. ANL-PHY-86-1, 1986 (unpublished).
[62]G. Auger, D. Jouan, E. Plagnol, F. Pougheon, F. Naulin, H. Doubre, and C. Grégoire, Z. Phys. A **321**, 243 (1985).
[63]H. Nifenecker, J. Blachot, J. Crançon, A. Gizon, and A. Lleres, Nucl. Phys. **A447**, 532c (1985).
[64]M. Blann, Phys. Rev. C **31**, 1245 (1985).
[65]H. Y. Han, K. X. Jing, E. Plagnol, D. R. Bowman, R. J. Charity, L. Vinet, G. J. Wozniak, and L. G. Moretto, Nucl. Phys. **A492**, 138 (1989).
[66]K. Grotowski, J. Ilnicki, T. Kozik, J. Łukasiak, S. Micek, Z. Sosin, A. Wieloch, N. Heide, H. Jelitto, I. Kiener, H. Rebel, S. Zagromski, and A. J. Cole, Phys. Lett. B **223**, 287 (1989).
[67]W. Mittig. A. Cunsolo, A. Foti, J. P. Wieleczko, E. Auger, B. Berthier, J. M. Pascaud, J. Québert, and E. Plagnol, Phys. Lett. **154B**, 259 (1985); F. Auger, B. Berthier, A. Cunsolo, A. Foti, W. Mittig, J. M. Pascaud, E. Plagnol, J. Québert, and J.

P. Wieleczko, Phys. Rev. C **35**, 190 (1987).
[68]W. W. Wilcke, J. R. Birkelund, H. J. Wollersheim, A. D. Hoover, J. R. Huizenga, W. U. Schreder, and L. E. Tubbs, At. Data Nucl. Data Tables **25**, 5 (1980).
[69]D. J. Parker, J. Asher, T. W. Conlon, and I. Nagib, Phys. Rev. C **30**, 143 (1984).
[70]M. Blann, Annu. Rev. Nucl. Sci. **25**, 123 (1975).
[71]J. Wilczyński, K. Siwek-Wilczyńska, J. Van Driel, S. Gonggrijp, D. C. J. M. Hageman, R. V. F. Janssens, J. Łukasiak, and R. H. Siemssen, Phys. Rev. Lett. **45**, 606 (1982).
[72]M. Blann, Phys. Rev. C **28**, 1475 (1983).
[73]M. Blann, T. T. Komoto, and I. Tserruya, Phys. Rev. C **40**, 2498 (1989); M. Blann (private communication).
[74]M. Blann and T. T. Komoto, Phys. Rev. C **24**, 426 (1981).
[75]M. Beckerman and M. Blann, Phys. Rev. C **17**, 1615 (1978).
[76]M. Beckerman and M. Blann, Phys. Rev. Lett. **42**, 156 (1979).
[77]R. J. Charity, M. A. McMahan, G. J. Wozniak, R. J. McDonald, L. G. Moretto, D. G. Sarantites, L. G. Sobotka, G. Guarino, A. Pantaleo, L. Fiore, A. Gobbi, and K. D. Hildenbrand, Nucl. Phys. **A483**, 371 (1988); R. J. Charity (private communication).
[78]L. G. Moretto, Nucl. Phys. **A247**, 211 (1975).
[79]A. J. Sierk, Phys. Rev. C **33**, 2039 (1986); K. T. Devies and A. J. Sierk, *ibid.* **31**, 915 (1985).
[80]R. Vandenbosch, in *Nuclear Physics with Heavy Ions,* edited by P. Braun-Munzinger, Nuclear Science Research Conference Series, Vol. 6 (Harwood Academic, New York, 1984), p. 447.
[81]C. Grégoire and F. Scheuter, Phys. Lett. **146B**, 21 (1984).
[82]L. Pieńkowski, A. Lleres, H. Nifenecker, J. Blachot, J. Crançon, A. Gizon, M. Maurel, and C. Ristori, Z. Phys. A **334**, 315 (1989).
[83]J. B. Natowitz, S. Leray, R. Lucas, C. Ngo, E. Tomasi, and C. Volant, Z. Phys. A **325**, 467 (1986).
[84]C. Grégoire, B. Remaud, F. Sebilles, L. Vinet, and Y. Rattray, Nucl. Phys. **A465**, 317 (1987).
[85]G. F. Bertsch, H, Krause, and S. Das Gupta, Phys. Rev. C **29**, 673 (1984).
[86]E. Suraud (private communication).
[87]M. B. Tsang, G. F. Bertsch, W. G. Lynch, and M. Tohyama, Phys. Rev. C **40**, 1685 (1989).